Neuron-vascular Coupling in the Amygdala Control Behavioral State of Stress-induced Defecation and Innate Fear Retention

Jiayu Ruan[1,2,3,4], Huiqi Xie[1,2,3,4], Xinghua Quan[2,3,4], Yiyi Zhang[1,2,3,4], Dongdong Zhang[2,3,4], Wentao Wang[2,3,4], Jie-Min Jia[1,2,3,4, *]

Affiliations

1. College of Life Sciences, Zhejiang University, Hangzhou, Zhejiang 310058, China.
2. Key Laboratory of Growth Regulation and Translational Research of Zhejiang Province, School of Life Sciences, Westlake University, Hangzhou 310024, China.
3. Westlake Laboratory of Life Sciences and Biomedicine, Hangzhou 310024, China.
4. Laboratory of Neurovascular Biology, Institute of Basic Medical Sciences, Westlake Institute for Advanced Study, Hangzhou 310024, China.

*Correspondence: Jie-Min Jia (jiajiemin@westlake.edu.cn)

Abstract

Proper cerebral function depends on intact neurovascular coupling (NVC), a conservative biological process in mammals that can effectively and spatiotemporally regulate cerebral blood distribution. The amygdala is a critical cerebral region for regulating emotion and stress-related behaviors. However, how NVC participates in advanced cerebral function and the consequences of NVC dysfunction in the amygdala remain unclear. The lack of cellular-specific transgenic models and non-specific drug administration mainly limited previous studies on NVC. Moreover, almost all papers take the function of hyperemia as the readout of NVC, but the advanced significance of functional hyperemia still needs to be discovered. Hence, the findings could have been more robust. In this study, we broadly used cellular-specific transgenic models to manipulate NVC and combined them with the chemogenetic strategy to reveal NVC-related cerebral advanced function. This study confirmed that GLRB loss in mural cells leads to NVC enhancement, the first report of a transgenic NVC enhancement model. Also, we are the first to use the transgenic model to clarify that COX-2 in neurons contributes to NVC regulation. The major work of this study is using arterial smooth muscle cells (aSMCs) NR2D conditional knockout model as a presentative NVC dysfunction model to find that NVC dysfunction in the amygdala context-dependently leads to shorter innate fear retention and increased stress-induced defecation. Through chemogenetic inhibition of neurons in the amygdala can correct increased stress-induced defecation in NVC dysfunction mice. Besides, during the behavioral assay, we first report the correlation pattern between pupil size and locomotion during the virtual predator stimulation. Last, we found that caldesmon is the downstream protein of NR2D in aSMCs to regulate NVC, and the interaction site of NR2D and caldesmon may become a drug target for NVC-initiated mental disorders.

Introduction

Neurovascular coupling (NVC), where corresponding changes in cerebral blood flow accompany changes in neural activity, is a universally conserved biological process among mammalians that can spatiotemporally regulate cerebral blood supply distribution(1). The amygdala is a crucial cerebral region that regulates emotional and stress-related behaviors cross species (2-5). One of the known applications of NVC is functional magnetic resonance

imaging (fMRI) (6), in which high levels of the blood oxygenation level-dependent (BOLD) signal mirrored with an increase in NVC are often repeatedly observed in some classic cerebral regions of patients with emotional disorders (7) such as in the amygdala of the fear-related post-traumatic stress disorder (PTSD) patients (8, 9).

The innate fear response is a complex emotional behavioral that helps organisms protect themselves from potential threats (10, 11). The amygdala is responsible for responding to potential threats in the environment, and it does so by activating a cascade of physiological and behavioral responses like fight or flight to avoid damage (12, 13). However, when the amygdala activation is abnormal, the excessive or weakened response to threat is harmful. Besides the innate fear response, several studies have explored the relationship between stress-induced defecation and the amygdala (14, 15). In the animal model, repeated OFT (16, 17) and wrap restraint (18) increased stress-induced defecation, and another study directly points out that restraint stress causes neuron activation in the amygdala (19). Moreover, a study examined the relationship between stress and bowel function in patients with irritable bowel syndrome (IBS), and researchers found that patients with IBS had increased activity in the amygdala during resting-state(20, 21).

The above evidence indicates that amygdala activation correlates with innate fear response and stress-induced defecation, but causality is unclear. Moreover, current studies usually use the variation of functional hyperemia as a readout of NVC, but how functional hyperemia controls advanced cerebral function is unknown. For instance, the impact of NVC dysfunction in the amygdala on innate fear response and stress-induced defecation remains unclear.

To answer these questions, we validate a series of cellular-specific transgenic models that can alter the extent of NVC. A representative example is NR2D, one of the non-core subunits of the NMDA receptor. Lack of NR2D in arterial smooth muscle cells (aSMCs) leads to attenuating phase NVC dysfunction and causes shorter innate fear retention time and increased stress-induced defecation. The abnormal increased stress-induced defecation was corrected in the NVC dysfunction mice by inhibiting the amygdala neurons by the chemogenetic strategy.

Besides, mural cell-specific expressed caldesmon was the downstream protein of NR2D in aSMCs for NVC regulation, and the interaction site of NR2D and caldesmon may be a potentially specific drug target for NVC-initiated mental disorders.

Materials and methods

Animal and animal care

All mice procedures complied with the Institutional Animal Care and Use Committee (IACUC) guidelines of the School of Life Sciences, Westlake University. All mice housed in Westlake University Laboratory Animal Resource Centre with standard animal rooms provided a 12 hours light/dark cycle at 25°C. No more than six mice were fed in each cage, and standard chow and water were provided to the mice *ad libitum*. All transgenic mice were listed in Table 1.

Cell culture

Surgical tweezers were used to quickly extract cortex of P0 anesthetized mice, and tissue was put into 10ml 0.25% Trypsin (Thermo Scientific, Cat# 25200072, USA) to digest tissue for 15min at 37°C. After that, the solution was added with 1ml FBS (Gibico, Cat# 10099, USA) and filtered by a 40μm filter (Falcon, Cat# 352340, CHN). Finally, centrifuged 1,600*g at 4℃ for 5min and cells were resuspended by 5ml SMCM (ScienCell, Cat# 1101, USA) in T25 flasks (Corning, Cat# 430639, USA).

TMX administration

1. Tamoxifen for mice

Tamoxifen (MCE, Cat# HY-13757A, USA) was dissolved in corn oil (Aladdin, Cat# C116023-500ml, CHN) and orally administrated to mice (10mg/ml, 200ul per mice per day). Postnatal day 5 (P5) *grin2d* conditional knockout infant mice got tamoxifen through breast milk. On the fifth day after the birth of infant mice, their mother was orally administrated with tamoxifen for four days. As for conditional knockout *acta2*, Tamoxifen was given from P21 to P24. Otherwise, tamoxifen was orally administered from P60 to P63.

2. Tamoxifen for cell culture (include cell sorting)

119 When cells reached approximately 80% full of the bottom surface of T25 flasks, tamoxifen was
120 dissolved in DMSO (Solarbio, Cat# D8371, CHN) to add into culture medium (final
121 concentration 5μM). After four-day culture, EGFP (Ai47) or Tdtomato (Ai14) in cells were
122 expressed. Cells were sorted by MA-900 (Sony, FCCF-MBR, JPN) to obtain EGFP-positive or
123 Tdtomato-positive cells. Sorted cells were cultured in SMCM for further assay. The purity of
124 cells sorted by the same method had been verified in the published paper (22).
125
126 *RNA scope in situ hybridisation*
127 Horizontal sections (15μm) of tamoxifen administrated *SMA-creER:Ai14* (for *grin2d*) or *Pdgfrβ-*
128 *creER:Ai14* (for *glrb*) mice brain slices were obtained by CM1950 (Lecia, Histo-CM1950, DEU).
129 All RNA scope *in situ* hybridisation productions were obtained from ACDbio, including RNAcope
130 Multiplex Fluorescent Reagent Kit v2 (ACDbio, Cat# 323100, USA), *grin2d* probe (ACDbio,
131 Cat# 425951-C3, USA), *grin1* probe (ACDbio, Cat# 431611, USA), and *glrb* probe (ACDbio,
132 Cat# 1225261-C1, USA). All operation followed the reagent instructions and the published
133 paper (23).
134
135 *RT-PCR*
136 After obtaining sorted EGFP/Tdtomato-positive aSMCs, cells were cultured in 6cm dishes
137 (Corning, Cat# 430166, USA) with SMCM. After cells reached around 90% density, Trizol
138 (Sangon Biotec, Cat# B511311-0100, CHN) was used for the RNA extraction. For brain tissue,
139 after mice were anesthetized, the cortex or cerebellum of the mice was directly taken out, and
140 TRIzol was used for RNA extraction.
141
142 After RNA extraction, concentrations were measured by NanoDrop™ One (Thermo Scientific,
143 Cat# 840-317400. USA), and all samples were reverse transcription to cDNA (50ng/μl) using
144 HiScript III 1st Strand cDNA Synthesis Kit (Vazyme, Cat# R312-02, CHN). For the Real Time
145 Polymerase Chain Reaction (RT-PCR), each reaction contained 10μl of Green Taq Mix
146 (Vazyme, Cat# P131-AA, CHN), 2μl of cDNA, 2μl of primer pairs (10μM), and 6μl of RNAase-
147 free water. Agarose gel electrophoresis used 2% agarose gel (BIOWESTE, Cat# 111860, ESP),
148 100bp maker (Tsingke, Cat#: TSJ100-100, CHN), and ran at 220V for 30min. RT-PCR gel

149 images were obtained by Tanon imager (Tanon, 1600 Geil imager, CHN). Primer pairs listed in
150 Table 2.
151
152 *Western-bolt*
153 For tissue sample collection, samples were ground together with RIPA (Thermo Scientific, Cat#
154 89901, USA) on ice for 30min. For cell samples, after cells reached around 90% density, the
155 RIPA was used for protein extraction on ice for 30min. Protease Inhibitor Cocktail (CWBIO,
156 Cat# CW22008, CHN) was added into RIPA to prevent protein enzymolysis. Then, samples
157 were centrifuged 12,000*g at 4℃ for 5min, and supernatant were collected. Concentrations of
158 proteins were measured by Micro BCA Protein Assay kit (CWBIO, Cat# CW2011S, CHN), and
159 all samples were boiled with SDS-PAGE loading buffer (CWBIO, Cat# CW0027S, CHN) for
160 10min at 100℃. 8% SDS-polyacrylamide electrophoresis gels were used for gel running, and a
161 protein marker (GenStar, Cat# M221-05, CHN) was used to identify the protein size. After 90min
162 gels running at 120V (80V for the first 30min), gels were transferred to 0.45μm PVDF
163 membranes (Millipore, Cat# IPVH00010, USA) at 400mA for 120min. After transfer, PVDF
164 membranes were blocked by 5% non-fat milk in 1X TBST buffer for 60min at room temperature
165 with a mild horizontal shake.
166
167 After the block, the first antibody diluted with 5% non-fat milk in 1X TBST buffer was used to
168 incubate the membrane overnight at 4℃ with a mild horizontal shake. After the first antibody
169 incubation, the membrane was washed by 1X TBST 10min (3 replicates). The corresponding
170 second HRP-conjugated antibody diluted with 5% non-fat milk in 1X TBST buffer was used to
171 incubate the membrane 45min at room temperature with a mild horizontal shake. After the
172 second antibody incubation, the membrane was washed by 1X TBST 10min (3 replicates). ECL
173 kits (Abbkine, Cat# BMU102-CN, CHN) and gel image system (GE, GEL Imaging System
174 AI680RGB v.2.0, USA) were used for exposure photography. Antibodies listed in Table 3.
175
176 *Immunofluorescence staining (IF)*
177 For tissue Immunofluorescence (IF) staining, briefly, after anesthesia, the mice were perfused
178 with cold 1X PBS (10ml) and cold 4%PFA in 1X PBS (10ml) through the left ventricle to empty

179 blood and fix tissue. Afterwards, tissue was extracted and fixed by 4% PFA in 1X PBS 6 hours
180 at 4℃. For MCA branches IF staining, after the fixation, MCA branches were carefully extracted
181 from the brain using surgical tweezers. Then, treated isolated MCA branches by 1% Triton X-
182 100 (Diamond, Cat# A110694-0500, CHN) with 2.5% Normal Goat Serum (Jackson
183 ImmunoResearch, Cat# 005-000-121, USA) in 1X PBS for one hour at room temperature. Then,
184 isolated MCA branches were rewashed three times by 1XPBS. For other tissue like brain and
185 peripheral organs, all organs were sliced into 50μm (Leica, Histo-VT1200S, DEU) after the
186 fixation, then the subsequent process was similar to that of isolated MCA branches.
187
188 For cultured cell immunofluorescence staining. After cells reached around 90% density, cells
189 were passed by into 12-well plates (Corning, Cat# 3515, USA) with glass slices (30k cells per
190 well). After cells in 12-well plates reached around 70% density, cells in glass slices were fixed
191 by 4%PFA in 1X PBS for 10min at room temperature. Washed cell slices with 1X PBS 10min
192 (3 replicates), treated cells with 0.3% Triton X-100 in 1X PBS for 10min at room temperature,
193 and then washed again with 1X PBS 10min (3 replicates). Next, 5% BSA in 1X PBS was used
194 to block cell slices for 30min at room temperature. After the block, cell slices were rewashed as
195 described above.
196
197 In the staining process, the first antibody diluted with 1% BSA+0.1% Triton X-100 in 1X PBS
198 was used to incubate samples overnight at 4℃. After the first antibody incubation, samples
199 were washed with 1X PBS 10min (3 replicates). The corresponding donkey-source second
200 fluorescence-conjugated antibody diluted with 1% BSA+0.1% Triton X-100 in 1X PBS was used
201 to incubate samples 120min at room temperature. After the second antibody incubation,
202 samples were washed with 1X PBS 10min (3 replicates). After that, 1000X diluted Hoechst
203 (AbMole, Cat# M5112, CHN) was used for nucleus staining (5min). Finally, tissue slices and
204 cell culture slices were covered by a glass slice with the mounting medium (SouthernBiotech,
205 0100-01, USA). Zeiss LSM800 (Zeiss, LSM800, DEU) microscopy was used for photography.
206 Antibodies listed in Table 3.
207
208 *Whisker stimulation*

209 The whisker was trimmed to only remain lane three and lane four on one side of the face. On
210 the day of the assay, mice were anesthesia with 1% pentobarbital sodium, and stable fixated
211 on the platform. The electro-motor-driven brush stimulated the whisker for 1 minute at 12Hz.
212 The principle of laser speckle contrast imaging has been described in the previous paper (24),
213 and the operation referred to the published paper (25). Laser Speckle Image System (RWD,
214 RFSLI ZW/RFSLI III, CHN) was used to monitor the CBF variation in the ROI of the opposite
215 barrel cortex of mice. The recording parameters were: 512*512 resolution, 10FPS, and 2min
216 recording.
217
218 *Vasomotion measurement*
219 Two weeks before the assay, a head fixator was placed on the head of the mouse, and a glass
220 cranial window replaced the 3-mm round skull above the cortex. On the day of the assay,
221 isoflurane (RWD, cat# R510-22-10, CHN) was used to anesthetize mice and RhoB dextran
222 (sigma, cat#r9379, 10mg/ml) was injected into the orbit. The mice were then fixed under a two-
223 photon microscope and recorded while awake. The image and analysis strategy were
224 consistent with our pre-print paper (doi: https://doi.org/10.1101/2023.11.05.565680).
225
226 *Immunoprecipitation assay*
227 Sorted Tdtomato-positive aSMCs were used for lentivirus infection and further
228 immunoprecipitation (IP) assay. Cells were cultured in 6cm dishes with SMCM. After cells
229 reached around 90% density, add lentivirus (Lenti-EF1-EGFP-CMV-grin2d-3XFlag-WPRE) into
230 the culture and keep for one week (virus titer: 2.6*109) for cells to over express NR2D. MA-900
231 sorted out EGFP and Tdtomato double-positive cells, and these cells were lentivirus-infected.
232 These cells were then cultured in 10cm dishes. After cells reached around 90% density, cells
233 were collected by RIPA reagent. The Protein G Magnetic beads kit (Epizyme, Cat# YJ002, CHN)
234 was used for the immunoprecipitation assay. NR2D antibody and IgG control antibody were
235 mixed with Protein G Magnetic beads respectively to pull down NR2D and its related protein.
236 Pull-down products were verified by western-bolt and analyzed through mass spectrometry.
237 Antibodies listed in Table3.
238

239 *cald siRNA interference*

240 All operations were followed by paper *Cannula Implantation into the Cisterna Magna of Rodents*
241 (https://doi.org/10.3791/57378). cald siRNA (1ul, 1nM) was mixed with Fluorescein
242 Isothiocyanate (FITC) (10mg/ml, Sigma, FD40S-1G, USA) for injection (20μl/10min). Ten
243 minutes after the injection, the scalp was removed, and the microscope was used to detected
244 the FITC signal (Zeiss, Axio Zoom v16, DEU). Only successfully injected mice remain. The
245 whisker stimulation was performed 48 hours after the injection, and brain was extracted for
246 Immunofluorescence staining and RT-PCR after the whisker stimulation.

247

248 *Looming assay*

249 This assay was carried out in a 35cm*35cm OFT box. Setting of the assay referred to the
250 published paper (26). Modifications include: 1. mice will be put in the OFT box to adapt for 10
251 minutes before starting the assay. 2. We only use a single camera at the top of the box to record.
252 3. We stimulate the mice when they move and are not close to the box wall rather than
253 continuously stimulating them. Each mouse performs three stimulations. 4. Locomotion speed
254 index before (LSI_{before}) calculation used the mean of locomotion from -30s to -10s and the mean
255 of locomotion from 0s to 3s; LSI_{after} calculation used the mean of locomotion from 0s to 3s and
256 the mean of locomotion from 3s to 30s. After the assay, mice were fed alone in a clean new
257 home cage for 90 minutes and then brain was extraction to detect c-fos expression in the
258 amygdala.

259

260 *VR assay*

261 This assay referred to a published paper (27). Two weeks before the assay, the mouse head
262 was fixed with a fixator. One week before the assay, the mice received 10 minutes of adaptive
263 training on the vital reality (VR) system every day (refers Figure 3B). On the day of the assay,
264 the mice were fixed on the VR system and given 5 minutes of adaptation. The screen in front
265 of the mouse will always play the landscape video unless it is stimulated. The stimulation video
266 was 3 seconds with the eagle swooped down, and the voice of the eagle played at the beginning
267 of the stimulation. There were 5 times of stimulation in total, and the criterion for the first
268 stimulation was that the mice moved for the first time after 5 minutes of adaptation. The criteria

269 for subsequent stimulation were that the last stimulation ended for at least 2 minutes and the
270 mice resumed movement. The assay stopped 2min after the last stimulation. The pupil size
271 variation, locomotion speed, defecation and urination of mice were recorded during the whole
272 assay. After the assay, mice were fed alone in a clean new home cage for 90 minutes and then
273 brain was extraction to detect c-fos expression in the amygdala.
274
275 *Cat video stimulation assay*
276 The assay was carried out in a 40cm*40cm OFT box. The mouse head was fixed with a fixator
277 on the head two weeks before the assay. One week before the assay, the mice received 10
278 minutes of adaptive training on the treadmill. On the day of the assay, the mice were fixed on
279 the treadmill, and played the video of cat hunting on the iPad Air (Apple, Cat#: 3rd generation,
280 USA) in front of the mouse (16cm) three trails for stimulation (30s for each trail). One trail
281 contains 10s empty, and 20s cat appearance (cat ambush at 26s). The camera above the box
282 was used for recording in the assay.
283
284 *CD-1 fear assay*
285 The setup of CD-1 fear assay referred to published papers(28-31). Aggressive CD-1 mice that
286 were never exposed to NVC dysfunction and control mice (described as B6 mice below) were
287 used for the assay. Before the assay, simultaneously put a single B6 mouse and a CD-1 mouse
288 into a home cage. The cage contains new padding and a metal lid on the top. One side of the
289 metal lid is used for placing food and water bottles, so the height is lower than another side.
290 After that, the camera was used to record all behaviours of B6 mice and CD-1 mice in 10
291 minutes. After the assay, CD-1 and B6mice were separated again. After the assay, B6 mice
292 were fed alone in a clean new home cage for 90 minutes and then brain was extraction to detect
293 c-fos expression in the amygdala.
294
295 *Home cage physical examination*
296 The blood pressure of mice was measured by Kent Noninvasive blood pressure measurement
297 system for animals/Biopac physiological signal analytical system (Kent/Biopac, Cat#, USA)
298 before the mice were put into the home cage. Each home cage only contains four mice. In each

cycle (three days), 60g of food, 340g of water (including bottle weight), and 100g of padding were provided. Food/water consumption, weight of mice, fecal particles, and urination amount (counted by increased padding weight) were measured at the end of each cycle. Three cycles of monitoring were performed for each home cage.

Chemogenetic manipulation

2.88^{E+12}VG/ml AAV2/9-mCaMKIIa-hM3D(Gq)-mCherry-ER2-WPRE-pA (Shanghai Taitool Bioscience Co., Ltd, CHN) was used for chemogenetic manipulation. Bilateral amygdala injection (150nl each side, AP: -1.6mm; ML: +/-3.45mm; DV: -4.1mm) was performed two weeks before the assay. Intraperitoneal injection of DREADD agonist 21 (C21, MCE, Cat# HY-100234, USA) was used to inhibit neurons in the amygdala. The injection strategy referred a published paper (32).

Open field test

The setup of open field test (OFT) referred to published papers (33-36). Each mouse was placed in the central area of a 40*40 cm or 35*35 cm box for the OFT. The camera recording was 15 minutes. For chemogenetic manipulation assay, only use 40*40 cm box for OFT, and C21 injection was 45min before the OFT.

Open field-like test

The setup of open field-like test (OFLT) referred to published paper (29). Each mouse was placed in the central area of a 23*23 cm box for the OFLT. An iron mesh wall replaced one wall of the box. Sketch paper was put on the bottom of the box to collect urine. Symmetric space is on the opposite side of the iron mesh wall. The camera recording was 20 minutes. For the analysis, the box was divided into three parts (left area, central area, and right area) to analyze the preference of mice for iron mesh wall (right area close to the iron mesh wall).

Tube stress

The tube stress assay refers to published papers (37-39). 50ml tube were used to restrain the mice. The tube cap and tube surface will be drilled to ensure normal breathing of mice. Mice

329 were restrained in the tube for 15min, and then calculate the fecal production. For
330 chemogenetic manipulation assay, The tube stress assay was performed 45min after C21
331 injection.
332
333 *Mice quarantine assay*
334 Mice were intraperitoneal C21 injection at the beginning of the assay, and then each mouse
335 was isolated into a clean cage without water, food, and padding supply for 1 hour. Defecation
336 and urination results were checked at the end of assay.
337
338 *Electrophysiology*
339 Parameter settings of the Electrophysiology followed the published paper (40). Mice were
340 anaesthetized and then perfused with 10ml cold artificial cerebrospinal fluid (aSCF). Then, the
341 brain was extracted and put into chilled aCSF. 300μm Brain slices were prepared in coronal
342 sections (Leica, Histo-VT1200S, DEU). Then, brain slices were transferred to aCSF at 34 °C
343 for 30 minutes and then recovered to room temperature for one hour. All solutions were
344 oxygenated with 95% O2 + 5% CO2. For *in vitro* electrophysiological recording of the amygdala
345 neurons, currents were measured under whole-cell patch-clamp recordings using pipettes with
346 a typical resistance of 5–6 MΩ filled with an internal solution. Cells were visualized by
347 microscope. The recording system includes an amplifier (MultiClamp 700B) driven by
348 Axon™pCLAMP™ (v.10.7) and a digital-to-analog converter (Digidata 1550B). The resting
349 membrane potential (RMP) was determined during the silent period of neuronal spontaneous
350 activity. Then, continuously increasing stimulation current was given from -20pA to 300pA
351 (lasting one second), and the number of action potentials (AP) was recorded in different levels
352 of current stimulation.
353
354 *Statistical analysis software and code*
355 All the analysis of fluorescence intensity and grey value used Zeiss Zen Lite (v2.3) and ImageJ
356 (v1.53u). All whisker stimulation original data were measured by LSIS-self software (v5.0).
357 Parameters “Time to peak”, “Peak mean”, “Peak maximum”, “OFLT heat map”, “Z-score cross
358 area” and data inclusion criteria before bioinformatics analysis of mass spectrometry data were

359 calculated using self-compiled MATLAB codes. KEGG and GO analysis referred to DAVID
360 Bioinformatics Resources (https://david.ncifcrf.gov/home.jsp) and Kyoto Encyclopedia of
361 Genes and Genomes (https://www.genome.jp/kegg/). The c-fos expression distribution map
362 and KEGG pathway made by self-compiled R code. All the original behavioral data of OFLT
363 were recorded using any-maze (v4.73). OFT original behavioral data were recorded using
364 Noldus. The implementation of Looming stimulation assay and VR stimulation assay including
365 raw data collection were assisted by BAYONE Co., Ltd. All statistical data were processed by
366 Numbers (v12.2), and all figures were made by Prism (v9.4.1).
367

368 **Results**

369 *Neurotransmitter receptors loss in mural cells lead NVC dysfunction*

370 Under physiological conditions, sustained and correct neuronal activation in cerebral regions,
371 including the amygdala, requires normal functioning of NVC (41-43). Therefore, we first plan to
372 validate the ability of some *de novo* and classic potential candidates on NVC and then to see
373 the impact of NVC dysfunction on particular advanced functions of neural circuits.
374

375 Our previous study reported that NR1 (encoded by gene *grin1*), the core subunit of NMDA
376 receptor encoded by gene *grin1* in aSMCs, regulates NVC, but the contribution of another non-
377 core subunit is still unclear. Hence, we first detected the expression level of all NMDA receptors
378 in cerebral aSMCs to map the expression pattern of NMDA receptors. Among the seven known
379 NMDA receptors, we found that apart from NR1, only the non-core subunit NR2D (encoded by
380 gene *grin2d*) can be detected (Figure 1A/B). This result suggests that the NMDA receptor in
381 cerebral aSMCs may only be composed of NR1 and NR2D.
382

383 Based on the above results, the loss of NR2D in aSMCs may share the same consequence of
384 NR1 loss. Therefore, we further validated the expression of *grin2d*/NR2D in cerebral smooth
385 muscle cells and other organs (Figure 1C/D, Figure S1E/H). Then, we confirmed the genetic
386 tool (cre-loxp system) was specific and efficient in manipulating the gene expression (Figure
387 1D/E/F/G/H/I/K, Figure S1F/G), and conditional knockout *grin2d* in aSMCs did not impact the
388 maker protein expression of SMCs (Figure 1J/L).

389

390 Afterwards, we conducted the whisker stimulation to evaluate the NVC reflected by the ability
391 of functional hyperemia in our transgenic mice (Figure 1M). First, we confirmed that multiple
392 consecutive whisker stimulations did not impact the data on repeatability and reliability (Figure
393 S1A/C), and Tamoxifen administration did not impact functional hyperemia (Figure S1B/D).
394 Based on the above, data showed that specific *grin2d* loss in aSMCs (driven by SMA-creER)
395 can attenuate functional hyperemia, and this reduction is independent of the time of knocking
396 out *grin2d*, which indicates that the functional compensation from other non-core subunits of
397 NMDA receptors in aSMCs may not exist (Figure 1N/O). In addition, *grin2d* loss throughout all
398 mural cells (driven by Pdgfrβ-creER) rather than limited to aSMCs revealed a similar
399 aggravated inhibition of functional hyperemia, suggesting that mural cells other than aSMCs
400 may not express *grin2d*. Knocking out *grin2d* alone in aSMCs is enough to produce significant
401 functional hyperemia inhibition (Figure 1N/O). Finally, the double knockout of *grin1* and *grin2d*
402 in aSMCs is similar to those of a single knockout of *grin1* or *grin2d*, suggesting that *grin1* and
403 *grin2d* in aSMCs regulate the functional hyperemia in the same pathway (Figure 1N/O).
404

405 To verify the downstream pathway of NR2D regulating neurovascular coupling in aSMCs, we
406 identified the proteins interacting with NR2D by immunoprecipitation. The Vascular smooth
407 muscle contraction pathway, identified through KEGG Pathway Enrichment, contains
408 caldesmon and smooth muscle actin (SMA) (Figure S2A/G). SMA is the final executive protein
409 responsible for cell contraction and relaxation (44). Non-phosphorylated caldesmon binds with
410 actin and myosin to prevent their interaction, thereby inhibiting the contraction of the cell
411 skeleton (45-48). Through phosphorylation of MAPK (49) and PAK (50) or binding with calcium-
412 activated CaM (51), caldesmon is removed from the binding site of actin and myosin, leading
413 to the contraction of the cytoskeleton. First, we conditional knockout *acta2* (gene name of SMA)
414 in mural cells (Figure S2E) and found that functional hyperemia was inhibited (Figure S2H/I).
415 These results suggest that SMA is involved in regulating NVC. Directly affecting contraction
416 and relaxation machines of mural cells could impact NVC. As for caldesmon, this protein almost
417 mural cells specific in the brain. So, we block the expression of caldesmon in the whole brain
418 by injecting *cald* (gene name of caldesmon) siRNA into the cisterna magna. After 48 hours of

419 siRNA interference, we found that the expression of caldesmon decreased (Figure S2B/C/D/F)
420 and functional hyperemia in mice was inhibited at the same time (Figure S2H/I), suggesting
421 that caldesmon may participate in the regulation of nNVC as the downstream of NR2D. In
422 conclusion, caldesmon and SMA potential are downstream proteins of NR2D in aSMCs.
423
424 In addition to the NMDA receptor, we verified the contribution of GLRB and COX-2 in NVC.
425 Firstly, we found that GLRB (encoded by gene *glrb*), the beta subunit of the glycine receptor,
426 was also expressed in cerebral mural cells. The expression of *glrb*/GLRB is relatively
427 concentrated in venous smooth muscle cells (vSMCs) and less in aSMCs and pericytes (Figure
428 1P/R/S). Functional hyperemia can be enhanced when *glrb* lost in all mural cells (Figure 1N/O).
429 This phenomenon was the first reported example of NVC enhancement by the trangenetic
430 model rather than chemical drugs. Besides, we also found that *glrb* loss in mural cells impacts
431 the vasomotion (Figure S1I). Although the vasomotion frequency did not vary in veins, the
432 vasomotion amplitude increased. However, only conditional knockout *glrb* in aSMCs did not
433 impact the frequency and amplitude of venous vasomotion (Figure S1J/K). These data indicate
434 that *glrb* expressed on vSMCs was critical in inhibiting functional hyperemia and venous
435 vasomotion amplitude. This suggests that vasomotion variations may correlate with NVC
436 variations, but the causality is unknown.
437
438 As for COX-2 (encoded by the gene *ptgs2*), the previous view was that COX-2 mainly
439 expressed in neurons, and total COX-2 knockout or drug inhibition can inhibit functional
440 hyperemia by approximately 50% (52). However, we also found that COX-2 was also expressed
441 in cerebral aSMCs (Figure 1Q/T). To clarify the contribution of COX-2 in different types of cells,
442 we conditional knock out *ptgs2* in neurons (driven by Emx1-cre) and aSMCs (driven by SMA-
443 creER). Data showed that specific knockout of *ptgs2* in aSMCs did not affect functional
444 hyperemia. However, in neurons, it reduced by approximately 50%, indicating that COX-2
445 expressed in aSMCs was not involved in regulating functional hyperemia, and the significant
446 contribution came from COX-2 in neurons (Figure 1N/O).
447
448 *NVC dysfunction mice had shorter innate fear retention during the looming stimulation assay*

Looming stimulation assay is a classic model that reflects the innate fear response of mice, so we chose this classic model to detect the innate fear response ability of NVC dysfunction mice (Figure 2A). We characterized the locomotion of mice in the 30s before and after stimulation (Figure 2B). First of all, we detected no difference in the locomotion between NVC dysfunction mice and control mice during the non-stimulation period (-30s to -10s), which indicated no difference in the motor function of mice (Figure 2C). The difference in the possible locomotion data after stimulation did not come from the motor dysfunction of mice. After that, we evaluated the latency of the locomotion of mice return to the mean locomotion before the stimulation (-30s to -10s). We found that the latency of NVC dysfunction mice was shorter, which was more evident in the first two trials (Figure 2D). After that, we calculated the LSI of three trials (Figure 2E) and found that the LSI of NVC dysfunction mice after stimulation was significantly higher than that of control mice (Figure 2F). In addition, the Area Under Curve (AUC) of locomotion between 6s to 24s in NVC dysfunction mice was larger than that of control mice in the first trial (Figure 2G). The above data showed that NVC dysfunction had shorter innate fear retention. Finally, we detected the activation of neurons in the amygdala of mice after the assay, and found that the activation of neurons in NVC dysfunction mice decreased significantly (Figure 2H/I). This evidence suggests that the low-level activation of amygdala neurons was correlated to the shorter innate fear retention.

NVC dysfunction mice had shorter innate fear retention during the VR stimulation assay

To further simulate the real natural predators attack, we further used the VR system (Figure 3A/B) to give mice more real threaten to induce more real innate fear behaviour of mice. We analysed the data for 30s before and after each stimulation (Figure 3C). We first analysed the changes in pupil diameter and locomotion speed of mice from -30s to -10s in 5 trials. We found no difference in these two parameters between the NVC dysfunction mice and control mice (Figure 3E/F). The above evidence indicates that NVC dysfunction mice did not exhibit pre-existing abnormalities in pupil and locomotion before stimulation.

Afterwards, we used the Z-score to compare the pattern of mouse pupil diameter and locomotion of mice to analyze the correlation between these two diameters in 5 trials. In the

range of -3s to 0s, due to the onset of movement, the pupil diameter increases synchronously with the increase of locomotion speed, showing a positive correlation consistent with previous papers. In the range of 0s to 3s, the pupil diameter of mice will rapidly expand due to the stimulation. However, mice will also exhibit a freezing pattern, causing a rapid decrease in locomotion speed, resulting in a negative correlation between pupil diameter and locomotion speed. This pattern shift remained consistent across five trials (except for trial_4 in the NVC dysfunction group, where there was no difference). In summary, a positive correlation exists between pupil diameter and locomotion speed during normal movement in mice, and a negative correlation between them during mice were shocked (Figure 3D). This assay was the first one to characterize the correlation between pupil size and locomotion speed in mice during the virtual predator stimulation.

Next, we analysed the amplitude of pupil diameter changes in 5 trials, and there was no difference in the increase in pupil diameter between the NVC dysfunction mice and the control mice during the stimulation period (0s-3s) (Figure 3G). However, after the stimulation (4s-10s), the NVC dysfunction group mice had a faster rate of pupil shrinkage, especially in trial_2, where the pupil diameter of the NVC dysfunction mice decreased significantly than that of the control mice (Figure 3H). In addition, we also analysed the changes in the locomotion speed of mice during the stimulation period (0s-3s). In trail_1, the NVC dysfunction mice showed a lower locomotion speed decrease than the control mice (Figure 3I). After the VR stimulation assay, we analysed the activation of amygdala neurons in mice and found that the activation of amygdala neurons was lower in NVC dysfunction mice (Figure 3K/L). Based on the above results, it is suggested that the NVC dysfunction group had a shorter fear retention time and weaker instinctive fear response when the virtual predator attacked due to the less neuron activation in the amygdala.

Finally, we analysed the area enclosed by the z-score curve of mouse pupil diameter and locomotion speed during and after stimulation to reflect the adaptability of mice to continuous stimulation. We found that the area decreased with increasing repeats of stimulation in both groups of mice, indicating that the mice showed adaptability to continuous non-invasive

stimulation (Figure 3J/M).

NVC dysfunction mice had weaker innate fear response during the cat video stimulation

As a supplement to the looming and VR assay, to increase dimensions to verify whether the NVC dysfunction in the amygdala affects innate fear behaviours, we used the cat video as a visual trigger to stimulate the innate fear behaviour of mice. We used the retreat pattern (move backward) and tail rattling to evaluate the ability of innate fear response.

Firstly, we mapped the standing and retreating patterns of mice on the treadmill (Figure S3A). Firstly, we counted the number of tail rattling, which was positively correlated with the degree of fear level. It can be seen that the number of tail rattling in the NVC dysfunction mice was significantly lower than that in the control mice in the first trial (Figure S3B/C). Then, the number of tail rattling decreased in the following two trails, showing an adaptation trend. As for the retreat, it can be seen that compared with the control mice, NVC dysfunction mice had significantly less time to retreat at the stage of cat appearance and cat ambush, which was reflected in the probability and total time to retreat. However, with the increase of trials, the response of mice to the video weakened, showing a trend of adaptation (Figure S3D). The above data showed that NVC dysfunction mice had shorter innate fear retention, indicating that NVC dysfunction can affect the innate fear response in mice.

NVC dysfunction mice had weaker innate fear response during the CD-1 fight assay

In the above assay, we administered non-contact stimulation to mice to evaluate innate fear response. Next, we placed the NVC dysfunction mice in a cage with aggressive CD-1 mice for 10 minutes to observe the innate fear response in contact stimulation assay. We first map the fighting patterns of B6 mice with CD-1 mice in the cage (Figure S3E). Then, we analyzed the frequency of sniffing (Figure S3F). Results showed that the number of sniffing these between NVC dysfunction mice and control mice had no differences, indicating that the information input received by the two groups of mice was consistent. Therefore, the possible behavioural differences in the subsequent parameters do not originate from the information input bias due to NVC dysfunction.

Then, we found that compared with the control mice, the NVC dysfunction mice showed a significant reduction in the fight latency (Figure S3G), number of fights (Figure S3H), and total duration (Figure S3I). On the contrary, the NVC dysfunction mice spent longer in a narrow space than CD-1 mice (Figure S3J/O). In addition, we also analyzed the triggers and losers of each fight. Whether in the NVC dysfunction mice or the control mice, the main initiators of fights were CD-1 mice, but the rate of fights triggered by NVC dysfunction mice mildly increased (Figure S3K). As for fighting losers, we used flight behaviour as the index to identify the losers. CD-1 mice were nearly not defeated in the control mice group, but the probability of CD-1 defeat significantly increased in the NVC dysfunction group (Figure S3L). After the CD-1 fight assay, we measured the neuron activation in the amygdala and other cerebral regions (Figure S3M/N). Results showed that the activation of amygdala neurons in the NVC dysfunction mice was lower than in the control mice. Based on the above results, it can be concluded that in the contacted fight assay, NVC dysfunction mice showed similar shorter innate fear retention to that in the non-contact stimulation assay.

NVC dysfunction altered stress-induced defecation

We set up a series of assays from low-stress to high-stress levels to verify whether the NVC dysfunction will impact stress-induced defecation (Figure 4A). In the home cage with the lowest stress, there was no difference in the physiological and metabolic parameters between NVC dysfunction mice and the control mice, such as food (Figure 4C) /water (Figure S4A) intake, body weight (Figure S4D), blood pressure (Figure S4E), defecation (Figure 4B/D/E, and Figure S4B), and urination (Figure S4C). In addition, we also measured the intestinal system and found no difference in the length of intestines (Figure S4F), body weight (Figure S4G), and the rate between length and weight (Figure S4H) between the NVC dysfunction mice and the control mice. Also, intestinal bleeding cannot be detected in NVC dysfunction mice. After the home cage assay, brain was extracted from the mouse for the detection of neuron activation in the amygdala, and no obvious differences can be seen between NVC dysfunction mice and contril mice (Figure S4U).

In the electrophysiological recording of brain slices, the amygdala neurons of NVC dysfunction mice had similar minimum action potential activation current (Figure S4J), and resting-stage membrane potential (Figure S4K) were similar to that of control mice, and the ability of BLA neurons to generate action potentials during the different current stimulation was also normal (Figure S4L/M). These results confirm that the basic physical parameters and function of amygdala neurons were normal in NVC dysfunction mice.

In the Open Field Test (OFT), the fecal production of mice in the control group did not increase significantly at the 40cm OFT box compared with that in the home cage (Figure 4B). However, the defecation increased significantly after changing the OFT box to 35cm (Figure 4B), suggesting that space may induce stress in mice. Hence, subsequent assays were to increase the pressure by reducing the space. However, compared with the control group, the defecation of NVC dysfunction mice was significantly increased in two sizes of OFT boxes (Figure 4B/F/G), and NVC dysfunction mice produced more feces at each five minutes of OFT than that of control mice in the OFT (Figure S4I), which suggests that NVC dysfunction mice were more sensitive to increased stress. Furthermore, combining results obtained in the home cage and electrophysiological recording, it can be seen that increased stress-induced defecation in NVC dysfunction mice was context-dependent rather than the consequence of continuous defecation increase. Besides, we also found no difference in the running distance (Figure 4H) and area preference (Figure 4I) of the NVC dysfunction mice in the OFT—only the defecation-related parameters were altered, which showed that NVC dysfunction did not entirely change mice behaviors.

In addition, we also compared the stress-induced defecation in the OFT (40cm) in various NVC dysfunction mice (Figure S4N). In general, the number of fecal particles negatively correlated with the extent of functional hyperemia; that is, the decrease of functional hyperemia leads to an increase in defecation and vice versa. Importantly, *grin1* and *grin2d* conditional knock mice showed a similar increase in defecation, which is another dimension to indicate that they work in the same pathway. Besides, conditional knockout *ptgs2* in aSMCs did not affect functional hyperemia and defecation, while the conditional knockout *ptgs2* by Emx1-cre inhibited

599 functional hyperemia and increased defecation. Moreover, because the fecal production of mice
600 in the OFT is relatively low, *glrb* conditional knockout mice only exhibit defecation reduction in
601 the tube stress, which provides more space-induced stress to induce more stress-induced
602 defecation than the OFT. Based on the above, the increase in defecation may not be related to
603 a particular gene but to the alteration of NVC.
604
605 In the Open Field-like Test (OFLT), we modified the existing OFT paradigm to increase the
606 space-induced stress by narrowing the box size. The results showed that NVC dysfunction mice
607 produced more fecal particles than control mice (Figure 4B). Similarly, urination also increased
608 in the NVC dysfunction mice (Figure 4J, and Figure S4Q), and the increase near the iron mesh
609 wall was more prominent (Figure 4K, and Figure S4O), which was synchronous with the
610 increased preference of the right side of the box (Figure S4P/R/S/T), indicating that the
611 unknown space may attract mice and provide stress to mice at the same time. Due to this
612 phenomenon, the running distance of NVC dysfunction mice increased in the OFLT (Figure
613 S4R).
614
615 In the tube stress assay, mice were restrained in the tube, and there was no difference in
616 defecation between the NVC dysfunction mice and the control mice (Figure 4B). Still, the
617 defecation of the two groups increased significantly compared with that in the home cage and
618 the OFT, which showed that fecal production reached the maximum in this assay and more
619 stress can no longer make mice produce more feces. As mentioned above, conditional
620 knockout *glrb* in mural cells lead defecation decreased in the tube stress (Figure S4N).
621
622 To reveal the mechanism for the increase in defecation, we analyzed the activation of neurons
623 in different cerebral regions after the OFT. We found that neuron activations of NVC dysfunction
624 mice were almost attenuated or unchanged (Figure 4L/M/N). Only a few cerebral regions
625 showed increased neuron activation, including the amygdala (Figure S4V), which strongly
626 indicates that NVC dysfunction in the amygdala leads to abnormal neuron activation, which
627 may correlate with abnormal stress-induced defecation. Vascular anatomical evidence (Figure
628 S4W), including BOLD signal evidence, proved that the amygdala has abundant vascular

distribution, which is the structural cornerstone for NVC to affect the excitability of amygdala neurons. Further analyses confirmed that neurons activated by the OFT in the BLA were mainly excitatory neurons, and approximately 60% were excitatory neurons in CeA (Figure 4O). These proportions did not change in the NVC dysfunction mice, indicating that the defecation increase in the NVC dysfunction group was not due to extra circuit activation. However, the activation extent of the same circuits was different.

The ultimate executor of stress-induced defecation is undoubtedly neurons. Therefore, if the abnormal activation of amygdala neurons leads to increased stress-induced defecation in NVC dysfunction mice, the artificial reduction of neuron activation may correct the increase in abnormal feces. So, we used the chemogenetic method to inhibit the activation of amygdala neurons (Figure 4P) and found that the defecation of mice in quarantine assay (Figure 4Q), OFT (Figure 4R), and tube stress assay (Figure 4S) were significantly reduced. This decrease in defecation was also observed in the NVC dysfunction mice, suggesting that NVC dysfunction in the amygdala specifically leads to abnormally increased activation of excitatory neurons to enhance the stress-induced defecation, and this phenomenon could be corrected by directly inhibiting the neuron activation in the amygdala.

Discussion

In this study, we found three proteins (NR2D, GLRB, COX-2) involved in the regulation of NVC, in which the loss of GLRB in mural cells leads to the enhancement of NVC, which is the first reported transgenic model that can enhance NVC. Previous studies only reported that NVC was enhanced by drug inhibition. In addition, we also clarified the cellular identity of COX-2 regulating NVC. COX-2 is expressed in neurons, glial cells, and cerebral aSMCs. Previous studies have used total knockout mice to study the effect of COX-2 on NVC, but this model lacks cell specificity and produces serious side effects (53). Similarly, the assay of drug inhibition (like NS-398) on COX-2 cannot achieve cell specificity (52). In this study, we used Emx1-cre and SMA-creER mice, respectively, to distinguish the contribution of COX-2 in neurons and SMCs to NVC by transgenic strategies. Our conclusion confirmed that COX-2 expressed on neurons mainly mediated the regulation of NVC but not COX-2 in SMCs.

We selected NR2D conditional knockout mice as the representative NVC dysfunction model for further study. We found that the double knockout of NR1 and NR2D in SMCs would not further aggravate the effect of NVC. Besides, NR1 and NR2D single knockout mice showed similar increased stress-induced defecation. This evidence suggests that the non-core NMDA receptor subunit NR2D worked together with NMDA receptor core subunit NR1 in the same pathway. We have further broadened the field of NVC research because this study first reported the effect of NVC on advanced cerebral function, like stress-induced defecation and innate fear response. Previous NVC studies, whether using laser Doppler imaging (54), laser speckle imaging (55) or two-photon imaging (56), were limited to detecting functional hyperemia itself but not the consequence of abnormal functional hyperemia. These assays cannot reflect the changes in higher-level cerebral function during NVC dysfunction. This study found that NVC-attenuated mice showed abnormally increased stress-induced defecation and shorter innate fear retention under different stimulation models. It should be noted that there is no significant difference between NVC dysfunction mice and control mice in the home cage without stimulation, which indicates that NVC dysfunction is not obvious in the resting state. Only after stimulation can NVC dysfunction mice show abnormal advanced function, which may also be the difficulty in detecting NVC-related advanced function. The data from the electrophysiology confirmed that the function of neurons was normal in NVC dysfunction mice, and only in the activation degree to particular stimulation different from that of normal mice, which indicated that the cause of some diseases, such as IBS, might not be the lesion of neurons but the lesion of NVC of these neurons.

Therefore, NVC may become a potential candidate for mental diseases in the future, and NR2D expressed on cerebral aSMCs is an ideal target. We found that only cerebral aSMCs expressed NR2D in vascular SMCs. In addition, with the increase of age, the expression of NR2D in the whole brain decreases, which makes the side effects of drugs targeting NR2D in SMCs relatively low. More importantly, we found that caldesmon was downstream of NR2D by immunoprecipitation and functional hyperemia detection, while caldesmon is only expressed in mural cells in the brain. Suppose the drug candidate is designed to strengthen/block the

689 interaction between NR2D and caldesmon, in that case, the specificity of candidates will be
690 significantly improved because the interaction between NR2D and caldesmon exists only in
691 cerebral aSMCs. Hence, by targeting the interaction site of NR2D and caldesmon, the
692 candidate compound can correct the mental disorders initiated by NVC.
693

694 **Acknowledgement**

695 We thank Yanmei Tao for sharing *Nestin-cre* mice and *Emx1-cre* mice. We thank Bo Zhou for
696 sharing *SMA-creER* mice. We thank Zilong Qiu for sharing Ai47 mice. We thank Xiang Yu for
697 sharing *PdgfrβCreER* mice. We thank Yangang Sun for sharing *grin1* mice. We thank Woo-
698 Ping Ge for sharing Ai14 mice. We thank Yuxiao Niu for drawing KEGG pathway map. We thank
699 Jishuai Wang for electrophysiology recording. We thank Bingrui Zhao for cell sorting. We thank
700 Xu Hu for primer sequences sharing of NMDA receptors.
701

702 **Conflict of Interest**

703 We declare that we do not have any financial or personal relationships with other people or
704 organizations, which may affect our work inappropriately, and there are no professional or other
705 personal interests of any nature or kind in any products, services and/or companies. These
706 interests may be interpreted as affecting or reviewing the positions in the following manuscripts.
707

708 **References**

709 1. Drew PJ. Neurovascular coupling: motive unknown. Trends Neurosci. 2022;45(11):809-19.
710 2. Pitman RK, Rasmusson AM, Koenen KC, Shin LM, Orr SP, Gilbertson MW, et al. Biological
711 studies of post-traumatic stress disorder. Nat Rev Neurosci. 2012;13(11):769-87.
712 3. Whalen PJ, Kagan J, Cook RG, Davis FC, Kim H, Polis S, et al. Human amygdala
713 responsivity to masked fearful eye whites. Science. 2004;306(5704):2061.

714 4. Hadj-Bouziane F, Bell AH, Knusten TA, Ungerleider LG, Tootell RB. Perception of
715 emotional expressions is independent of face selectivity in monkey inferior temporal cortex.
716 Proc Natl Acad Sci U S A. 2008;105(14):5591-6.
717 5. Harris AP, Lennen RJ, Marshall I, Jansen MA, Pernet CR, Brydges NM, et al. Imaging
718 learned fear circuitry in awake mice using fMRI. Eur J Neurosci. 2015;42(5):2125-34.
719 6. Lacroix A, Toussay X, Anenberg E, Lecrux C, Ferreiros N, Karagiannis A, et al. COX-2-
720 Derived Prostaglandin E2 Produced by Pyramidal Neurons Contributes to Neurovascular
721 Coupling in the Rodent Cerebral Cortex. J Neurosci. 2015;35(34):11791-810.
722 7. Clemm von Hohenberg C, Weber-Fahr W, Lebhardt P, Ravi N, Braun U, Gass N, et al.
723 Lateral habenula perturbation reduces default-mode network connectivity in a rat model of
724 depression. Transl Psychiatry. 2018;8(1):68.
725 8. Ahmed-Leitao F, Spies G, van den Heuvel L, Seedat S. Hippocampal and amygdala
726 volumes in adults with posttraumatic stress disorder secondary to childhood abuse or
727 maltreatment: A systematic review. Psychiatry Res Neuroimaging. 2016;256:33-43.
728 9. Kamiya K, Abe O. Imaging of Posttraumatic Stress Disorder. Neuroimaging Clin N Am.
729 2020;30(1):115-23.
730 10. Coryell MW, Ziemann AE, Westmoreland PJ, Haenfler JM, Kurjakovic Z, Zha XM, et al.
731 Targeting ASIC1a reduces innate fear and alters neuronal activity in the fear circuit. Biol
732 Psychiatry. 2007;62(10):1140-8.
733 11. Misslin R. The defense system of fear: behavior and neurocircuitry. Neurophysiol Clin.
734 2003;33(2):55-66.
735 12. Davis M. NMDA receptors and fear extinction: implications for cognitive behavioral therapy.
736 Dialogues Clin Neurosci. 2011;13(4):463-74.
737 13. Shultz B, Farkash A, Collins B, Mohammadmirzaei N, Knox D. Fear learning-induced
738 changes in AMPAR and NMDAR expression in the fear circuit. Learn Mem. 2022;29(3):83-92.
739 14. Taguchi R, Shikata K, Furuya Y, Hirakawa T, Ino M, Shin K, et al. Selective corticotropin-
740 releasing factor 1 receptor antagonist E2508 reduces restraint stress-induced defecation and
741 visceral pain in rat models. Psychoneuroendocrinology. 2017;75:110-5.
742 15. Kakol-Palm D, Brusberg M, Sand E, Larsson H, Martinez V, Johansson A, et al. Role of
743 tachykinin NK(1) and NK(2) receptors in colonic sensitivity and stress-induced defecation in

744 gerbils. Eur J Pharmacol. 2008;582(1-3):123-31.
745 16. Candland DK, Nagy ZM. The open field: some comparative data. Ann N Y Acad Sci.
746 1969;159(3):831-51.
747 17. Archer J. Tests for emotionality in rats and mice: a review. Anim Behav. 1973;21(2):205-
748 35.
749 18. Suda K, Setoyama H, Nanno M, Matsumoto S, Kawai M. Involvement of parasympathetic
750 pelvic efferent pathway in psychological stress-induced defecation. World J Gastroenterol.
751 2013;19(8):1200-9.
752 19. Morgan A, Gaulden A, Altemus M, Williford K, Centanni S, Winder D, et al.
753 Cyclooxygenase-2 inhibition prevents stress induced amygdala activation and anxiety-like
754 behavior. Brain Behav Immun. 2020;89:513-7.
755 20. Qi R, Liu C, Weng Y, Xu Q, Chen L, Wang F, et al. Disturbed Interhemispheric Functional
756 Connectivity Rather than Structural Connectivity in Irritable Bowel Syndrome. Front Mol
757 Neurosci. 2016;9:141.
758 21. Yu Z, Liu LY, Lai YY, Tian ZL, Yang L, Zhang Q, et al. Altered Resting Brain Functions in
759 Patients With Irritable Bowel Syndrome: A Systematic Review. Front Hum Neurosci.
760 2022;16:851586.
761 22. Li X, Zhou L, Zhang X, Jin Y, Zhao B, Zhang D, et al. Proteins secreted by brain arteriolar
762 smooth muscle cells are instructive for neural development. Mol Brain. 2022;15(1):97.
763 23. Yu XD, Zhu Y, Sun QX, Deng F, Wan J, Zheng D, et al. Distinct serotonergic pathways to
764 the amygdala underlie separate behavioral features of anxiety. Nat Neurosci.
765 2022;25(12):1651-63.
766 24. Boas DA, Dunn AK. Laser speckle contrast imaging in biomedical optics. J Biomed Opt.
767 2010;15(1):011109.
768 25. Jin Y, Shi P, Wang Y, Li J, Zhang J, Zhao X, et al. Precise control of embolic stroke with
769 magnetized red blood cells in mice. Commun Biol. 2022;5(1):136.
770 26. Shang C, Chen Z, Liu A, Li Y, Zhang J, Qu B, et al. Divergent midbrain circuits orchestrate
771 escape and freezing responses to looming stimuli in mice. Nat Commun. 2018;9(1):1232.
772 27. Wang L, Chen IZ, Lin D. Collateral pathways from the ventromedial hypothalamus mediate
773 defensive behaviors. Neuron. 2015;85(6):1344-58.

774 28. Borelli KG, Blanchard DC, Javier LK, Defensor EB, Brandao ML, Blanchard RJ. Neural
775 correlates of scent marking behavior in C57BL/6J mice: detection and recognition of a social
776 stimulus. Neuroscience. 2009;162(4):914-23.
777 29. Arakawa H, Arakawa K, Blanchard DC, Blanchard RJ. Scent marking behavior in male
778 C57BL/6J mice: sexual and developmental determination. Behav Brain Res. 2007;182(1):73-9.
779 30. Arakawa H, Arakawa K, Blanchard DC, Blanchard RJ. A new test paradigm for social
780 recognition evidenced by urinary scent marking behavior in C57BL/6J mice. Behav Brain Res.
781 2008;190(1):97-104.
782 31. McQuaid RJ, Audet MC, Anisman H. Environmental enrichment in male CD-1 mice
783 promotes aggressive behaviors and elevated corticosterone and brain norepinephrine activity
784 in response to a mild stressor. Stress. 2012;15(3):354-60.
785 32. Khalil V, Faress I, Mermet-Joret N, Kerwin P, Yonehara K, Nabavi S. Subcortico-amygdala
786 pathway processes innate and learned threats. Elife. 2023;12.
787 33. Liu CY, Chen JB, Liu YY, Zhou XM, Zhang M, Jiang YM, et al. Saikosaponin D exerts
788 antidepressant effect by regulating Homer1-mGluR5 and mTOR signaling in a rat model of
789 chronic unpredictable mild stress. Chin Med. 2022;17(1):60.
790 34. Guo Z, Li S, Wu J, Zhu X, Zhang Y. Maternal Deprivation Increased Vulnerability to
791 Depression in Adult Rats Through DRD2 Promoter Methylation in the Ventral Tegmental Area.
792 Front Psychiatry. 2022;13:827667.
793 35. Kim S, Hong KB, Kim S, Suh HJ, Jo K. Creatine and taurine mixtures alleviate depressive-
794 like behaviour in Drosophila melanogaster and mice via regulating Akt and ERK/BDNF
795 pathways. Sci Rep. 2020;10(1):11370.
796 36. Lapmanee S, Charoenphandhu J, Teerapornpuntakit J, Krishnamra N, Charoenphandhu
797 N. Agomelatine, venlafaxine, and running exercise effectively prevent anxiety- and depression-
798 like behaviors and memory impairment in restraint stressed rats. PLoS One.
799 2017;12(11):e0187671.
800 37. Seo JS, Wei J, Qin L, Kim Y, Yan Z, Greengard P. Cellular and molecular basis for stress-
801 induced depression. Mol Psychiatry. 2017;22(10):1440-7.
802 38. Oh YS, Gao P, Lee KW, Ceglia I, Seo JS, Zhang X, et al. SMARCA3, a chromatin-
803 remodeling factor, is required for p11-dependent antidepressant action. Cell. 2013;152(4):831-

804 43.
805 39. Seo JS, Park JY, Choi J, Kim TK, Shin JH, Lee JK, et al. NADPH oxidase mediates
806 depressive behavior induced by chronic stress in mice. J Neurosci. 2012;32(28):9690-9.
807 40. Cui Y, Yang Y, Ni Z, Dong Y, Cai G, Foncelle A, et al. Astroglial Kir4.1 in the lateral habenula
808 drives neuronal bursts in depression. Nature. 2018;554(7692):323-7.
809 41. Lauritzen M, Dreier JP, Fabricius M, Hartings JA, Graf R, Strong AJ. Clinical relevance of
810 cortical spreading depression in neurological disorders: migraine, malignant stroke,
811 subarachnoid and intracranial hemorrhage, and traumatic brain injury. J Cereb Blood Flow
812 Metab. 2011;31(1):17-35.
813 42. Ruitenberg A, den Heijer T, Bakker SL, van Swieten JC, Koudstaal PJ, Hofman A, et al.
814 Cerebral hypoperfusion and clinical onset of dementia: the Rotterdam Study. Ann Neurol.
815 2005;57(6):789-94.
816 43. Pico-Perez M, Radua J, Steward T, Menchon JM, Soriano-Mas C. Emotion regulation in
817 mood and anxiety disorders: A meta-analysis of fMRI cognitive reappraisal studies. Prog
818 Neuropsychopharmacol Biol Psychiatry. 2017;79(Pt B):96-104.
819 44. Arnoldi R, Hiltbrunner A, Dugina V, Tille JC, Chaponnier C. Smooth muscle actin isoforms:
820 a tug of war between contraction and compliance. Eur J Cell Biol. 2013;92(6-7):187-200.
821 45. Kordowska J, Huang R, Wang CL. Phosphorylation of caldesmon during smooth muscle
822 contraction and cell migration or proliferation. J Biomed Sci. 2006;13(2):159-72.
823 46. Wang CL. Caldesmon and smooth-muscle regulation. Cell Biochem Biophys.
824 2001;35(3):275-88.
825 47. Hai CM, Gu Z. Caldesmon phosphorylation in actin cytoskeletal remodeling. Eur J Cell Biol.
826 2006;85(3-4):305-9.
827 48. Wang CL. Caldesmon and the regulation of cytoskeletal functions. Adv Exp Med Biol.
828 2008;644:250-72.
829 49. Childs TJ, Watson MH, Sanghera JS, Campbell DL, Pelech SL, Mak AS. Phosphorylation
830 of smooth muscle caldesmon by mitogen-activated protein (MAP) kinase and expression of
831 MAP kinase in differentiated smooth muscle cells. J Biol Chem. 1992;267(32):22853-9.
832 50. Foster DB, Shen LH, Kelly J, Thibault P, Van Eyk JE, Mak AS. Phosphorylation of
833 caldesmon by p21-activated kinase. Implications for the Ca(2+) sensitivity of smooth muscle

834 contraction. J Biol Chem. 2000;275(3):1959-65.
835 51. Janovick JA, Natarajan K, Longo F, Conn PM. Caldesmon: a bifunctional (calmodulin and
836 actin) binding protein which regulates stimulated gonadotropin release. Endocrinology.
837 1991;129(1):68-74.
838 52. Niwa K, Araki E, Morham SG, Ross ME, Iadecola C. Cyclooxygenase-2 contributes to
839 functional hyperemia in whisker-barrel cortex. J Neurosci. 2000;20(2):763-70.
840 53. Slattery P, Frolich S, Goren I, Nusing RM. Salt supplementation ameliorates
841 developmental kidney defects in COX-2(-/-) mice. Am J Physiol Renal Physiol.
842 2017;312(6):F1044-F55.
843 54. Li W, Prakash R, Chawla D, Du W, Didion SP, Filosa JA, et al. Early effects of high-fat diet
844 on neurovascular function and focal ischemic brain injury. Am J Physiol Regul Integr Comp
845 Physiol. 2013;304(11):R1001-8.
846 55. Remzso G, Nemeth J, Toth-Szuki V, Varga V, Kovacs V, Domoki F. NMDA attenuates the
847 neurovascular response to hypercapnia in the neonatal cerebral cortex. Sci Rep.
848 2019;9(1):18900.
849 56. Chow BW, Nunez V, Kaplan L, Granger AJ, Bistrong K, Zucker HL, et al. Caveolae in CNS
850 arterioles mediate neurovascular coupling. Nature. 2020;579(7797):106-10.
851

852 ## Figure legends

853 Figure 1. NR2D, GLRB, and COX-2 expression patterns and functional hyperemia ability
854 measurement of corresponding transgenic mice. A) Expression of all NMDA receptors in mRNA
855 level detected by RT-PCR. B) Statistical results of Figure 1A. Each dot indicates an independent
856 experiment, and the data are mean ± s.e.m. C) RNA scope results of *grin2d* expression in
857 cerebral aSMCs. Red arrow pointed out *grin2d* signal in aSMCs. The inserted histogram shows
858 the intensity of fluorescent signal. D) The WB and statistical results of NR2D in cerebellum of
859 P0 *grin2d f/f* mice, P60 grin2d f/f mice, and P0 *Emx1-cre:grin2d f/f* mice. Each dot indicates an
860 independent experiment, and the data are mean ± s.e.m. E) The WB and statistical results of
861 NR2D in cerebellum of P10 *grin2d f/f* mice, and P10 *SMA-creER:grin2d f/f* mice. Each dot
862 indicates an independent experiment, and the data are mean ± s.e.m. F) The RT-PCR and
863 statistical results of *grin2d* in cerebral aSMCs from *grin2d f/f mice*, and *SMA-creER:grin2d f/f*

mice. Each dot indicates an independent experiment, and the data are mean ± s.e.m. G) The WB and statistical results of NR2D in cerebral aSMCs from *grin2d f/f* mice, and *SMA-creER:grin2d f/f* mice. Each dot indicates an independent experiment, and the data are mean ± s.e.m. H) The top row: The IF results of NR2D in isolated MCA of *grin2d f/f mice* (left), and *SMA-creER:grin2d f/f mice* (right). The bottom row: The IF results of NR2D in cultured aSMCs from *grin2d f/f mice* (left), and SMA-creER:grin2d f/f mice (right). I) The statistical results of NR2D expression of the top raw in Figure 1H. Each dot indicates an independent experiment, and the data are mean ± s.e.m. J) The statistical results of smoothelin expression of the top raw in Figure 1H. Each dot indicates an independent experiment, and the data are mean ± s.e.m. K) The statistical results of NR2D expression of the bottom raw in Figure 1H. Each dot indicates an independent experiment, and the data are mean ± s.e.m. L) The WB and statistical results of SMA in the cortex of P60 *grin2d f/f* mice, P60 *SMA-creER:grin2d f/f* mice. Each dot indicates an independent experiment, and the data are mean ± s.e.m. M) Schematic diagram of blood flow increases in the ROI before, during, and after the whisker stimulation. N) CBF variation before, during, and after the whisker stimulation. The solid line indicates the mean value, and the dotted line indicates ± s.e.m. O) Statistical data of Figure 1N, including how long the CBF variation reaches the peak period and the mean CBF variation during the peak period. Each dot indicates a mean data from one mouse. Data are mean ± s.e.m. P) RNA scope results of *glrb* expression in cerebral mural cells (left), and GLRB expression in vSMCs. Q) The RT-PCR results of ptgs2 in cortex of P60 mice and aSMCs of cultured aSMCs (left). The IF results of COX-2 expression in cerebral aSMCs (right). R) Statistical results of RNA-scope in Figure 1P. Brain slices from 3 mice were analysed, and the data are mean ± s.e.m. S) Statistical results of IF in Figure 1P. Brain slices from 3 mice were analysed, and the data are mean ± s.e.m. T) Statistical results of RT-PCR in Figure 1Q. Each dot indicates a mean data from one mouse, and the data are mean ± s.e.m.

Figure 2. NVC dysfunction mice showed shorter innate fear retention in the looming assay. A) Schematic diagram of assay setting. B) Locomotion of mice around the stimulation in three trails (-30s to 30s). The solid line indicates the mean value, and the dotted line indicates ±

s.e.m. C) Locomotion of mice from -30s to -10s in three trails. Each dot indicates one mouse, and the data are mean ± s.e.m. D) Locomotion latency of mice, which means that how long the locomotion of the mouse return to the average locomotion from -30s to -10s. Each dot indicates one mouse, and the data are mean ± s.e.m. E) LSI of each mouse in three trails (from left to right). Each dot indicates one mouse. F) Statistical results of LSI_{after} of data in Figure 2E. Each dot indicates one mouse, and the data are mean ± s.e.m. G) Statistical analysis of the locomotion AUC in Figure 2B from 6s to 24s. Each dot indicates one mouse, and the data are mean ± s.e.m. H) Representative c-fos IF image in the amygdala. I) Statistical data of c-fos activation in Figure 2H. Each dot indicates one mouse, and the data are mean ± s.e.m.

Figure 3. NVC dysfunction mice showed shorter innate fear retention in the VR assay. A) Schematic diagram of assay setting. B) The structure of the VR system. C) Z-score of locomotion and pupil size of mice around the stimulation in five trails (-30s to 30s). D) The correlation between locomotion and pupil size from -3s to 0s and 0s to 3s. Each dot indicates one mouse, and the data are mean ± s.e.m. E) The pupil size of mice from -30s to -10s. Each dot indicates one mouse, and the data are mean ± s.e.m. F) The locomotion of mice from -30s to -10s. Each dot indicates one mouse, and the data are mean ± s.e.m. G) Statistical analysis of the pupil size AUC in Figure 3C from 0s to 3s. Each dot indicates one mouse, and the data are mean ± s.e.m. H) Statistical analysis of the pupil size AUC in Figure 3C from 3s to 10s. Each dot indicates one mouse, and the data are mean ± s.e.m. I) Statistical analysis of the speed AUC in Figure 3C from 0s to 3s. Each dot indicates one mouse, and the data are mean ± s.e.m. J) Statistical analysis of the curve enclosed area of pupil size and locomotion in Figure 3C from the first cross during the stimulation. Each dot indicates one mouse, and the data are mean ± s.e.m. K) Representative c-fos IF image in the amygdala. L) Statistical data of c-fos activation in Figure 3K. Each dot indicates one mouse, and the data are mean ± s.e.m. M) The presentative diagram of curve enclosed area of pupil size and locomotion shown in orange.

Figure 4. NVC dysfunction mice showed increased stress-induced defecation. A) Schematic diagram of assay setting from low stress to high stress. B) Fecal production in five assays

922 normalized in 15min. Each dot indicates one mouse, and the data are mean ± s.e.m. C) The
923 average food consumption of mice in the home cage. Each dot indicates one cage, and the
924 data are mean ± s.e.m. D) The average water consumption of mice in the home cage. Each dot
925 indicates one cage, and the data are mean ± s.e.m. E) The average fecal production number
926 of mice in the home cage. Each dot indicates one cage, and the data are mean ± s.e.m. F) The
927 defecation rate of mice in the OFT. Each dot indicates one mouse, and the data are mean ±
928 s.e.m. G) The defecation number of mice in the OFT. Each dot indicates one mouse, and the
929 data are mean ± s.e.m. H) The time of mice stay in the side of the box in the OFT. Each dot
930 indicates one mouse, and the data are mean ± s.e.m. I) The running distance of mice in the
931 OFT. Each dot indicates one mouse, and the data are mean ± s.e.m. J) The urination weight of
932 mice in the OFLT. Each dot indicates one mouse, and the data are mean ± s.e.m. K) The
933 urination mark size of mice in the OFLT. Each dot indicates one mouse, and the data are mean
934 ± s.e.m. L) Representative c-fos IF image in the amygdala. M) Statistical data of BLA c-fos
935 activation in Figure 4L. N) Statistical data of CeA c-fos activation in Figure 4L. O) Statistical
936 percentage of BLA /CeA c-fos and camKII double positive cells in all c-fos positive cells in Figure
937 4L. P) Schematic diagram of AAV2/5-mCaMKIIa-hM4D(Gi)-EGFP-ER2-WPRE-pA injection in
938 the amygdala (left). The c-fos activation pattern in the tube stress assay when I.P saline
939 (middle). The c-fos activation pattern in the tube stress assay when I.P C21 (right). Q) The fecal
940 production of amygdala-infected mice with/without C21 in the quarantine assay. Each dot
941 indicates one mouse, and the data are mean ± s.e.m. R) The fecal production of amygdala-
942 infected mice with/without C21 in the OFT. Each dot indicates one mouse, and the data are
943 mean ± s.e.m. S) The fecal production of amygdala-infected mice with/without C21 in the tube
944 stress assay. Each dot indicates one mouse, and the data are mean ± s.e.m.

945

946 Figure S1. Supplementary data of Figure1. A) CBF variation before, during, and after the
947 whisker stimulation. The solid line indicates the mean value, and the dotted line indicates ±
948 s.e.m. B) CBF variation before, during, and after the whisker stimulation with or without
949 tamoxifen administration. The solid line indicates the mean value, and the dotted line indicates
950 ± s.e.m. C) Statistical data of Figure S1A, including how long the CBF variation reaches the

951 peak period and the mean CBF variation during the peak period. Each dot indicates a mean
952 data from one mouse. Data are mean ± s.e.m. D) Statistical data of Figure S1A, including how
953 long the CBF variation reaches the peak period and the mean CBF variation during the peak
954 period. Each dot indicates a mean data from one mouse. Data are mean ± s.e.m. E) RNA-
955 scope data of grin1 and grin2d in cerebellum. F) IF of NeuN in the brains of *SMA-creER:Ai14*
956 mice. G) Statistical data in Figure S1F, and each dot indicates an data from one mouse, and
957 the data are mean ± s.e.m. H) IF of NR2D expression in heart, liver, spleen, lung, kidney, and
958 small intestine of *SMA-creER:Ai14* mice. The first row is zoom-out images of six organs, the
959 second row is zoom-in images of white circles in the first row, and the third row is histograms
960 of the red and green fluorescent intensities of the indicated sites in the second row.

961

962 Figure S2. Downstream signal pathways analysis of NR2D in aSMCs. A) WB results of
963 caldesmon detection in the IP product of NR2D. B) RT-PCR results of cald siRNA in whole brain
964 lysis. C) Statistics analyze of the bottom row in Figure S2A. Each dot indicates one mouse, and
965 the data are mean ± s.e.m. D) Statistics analyze of Figure S2F. Each dot indicate one mouse,
966 and the data are mean ± s.e.m. E) WB results of SMA expression in P60 *acta2 f/f* mice, and
967 p*dgfrβ-creER:acta2 f/f* mice. Each dot indicates one mouse, and the data are mean ± s.e.m. F)
968 IF results of caldesmon siRNA in the S1BF. G) KEGG pathway analysis of 915 proteins selected
969 from three independent mass spectrum data. H) CBF variation before, during, and after the
970 whisker stimulation. The solid line indicates the mean value, and the dotted line indicates ±
971 s.e.m. I) Statistical data of Figure S2H, including how long the CBF variation reaches the peak
972 period and the mean CBF variation during the peak period. Each dot indicates a mean data
973 from one mouse. Data are mean ± s.e.m.

974

975 Figure S3. NVC dysfunction mice showed attenuated innate fear resource in the cat video
976 stimulation assay and CD-1 fight assay. A) The locomotion pattern of mice in the treadmill of
977 three trials. B) Tail rattling times of mice. Each dot indicates one mouse, and the data are mean
978 ± s.e.m. C) Tail rattling rate of mice. D) The retreat times of mice. Each dot indicates one mouse,
979 and the data are mean ± s.e.m. E) The fight pattern of mice in the cage. F) Sniffing times of

980 mice. Each dot indicates one mouse, and the data are mean ± s.e.m. G) Fight latency of mice.
981 Each dot indicates one mouse, and the data are mean ± s.e.m. H) Number of fights happened
982 during the assay. Each dot indicates one mouse, and the data are mean ± s.e.m. I) Total fighting
983 times of mice. Each dot indicates one mouse, and the data are mean ± s.e.m. J) Time of B6
984 mice together with CD-1 mice in the narrow space. Each dot indicates one mouse, and the data
985 are mean ± s.e.m. K) Fighting trigger rate of mice. L) Fighting defeat (flight) rate of mice. M)
986 Statistical data of c-fos activation in Figure S3N. Each dot indicates one mouse, and the data
987 are mean ± s.e.m. N) Representative c-fos IF image in the amygdala. O) Example of fighting
988 cages.

989

990 Figure S4. Supplementary data of stress-induced defecation assay. A) The mean water
991 consumption of mice in the home cage. Each dot indicates one cage, and the data are mean ±
992 s.e.m. B) The mean fecal weight of mice in the home cage. Each dot indicates one cage, and
993 the data are mean ± s.e.m. C) The mean urine production of mice. Each dot indicates one cage,
994 and the data are mean ± s.e.m. D) The weight variation of mice during the home cage assay.
995 Each dot indicates one cage, and the data are mean ± s.e.m. E) The blood pressure of mice.
996 Each dot indicates one mouse, and the data are mean ± s.e.m. F) The weight of mice for
997 intestine analysis. Each dot indicates one mouse, and the data are mean ± s.e.m. G) The length
998 of intestine of mice. Each dot indicates one mouse, and the data are mean ± s.e.m. H) The ratio
999 of length and weight. Original data from Figure S4F/G. Each dot indicates one mouse, and the
1000 data are mean ± s.e.m. I)The defecation pattern of mice in OFT of every 5 minutes. Each dot
1001 indicates one mouse, and the data are mean ± s.e.m. J) The minimum current stimulation that
1002 can trigger AP. Each dot indicates one cells. Brain slices from 5 control mice and 5 NVC
1003 dysfunction mice. The data are mean ± s.e.m. K) The RMP of each neuron. Each dot indicates
1004 one cells. Brain slices from 5 control mice and 5 NVC dysfunction mice. The data are mean ±
1005 s.e.m. L) the current stimulation pattern. M) The number of APs in different current stimulation.
1006 Each dot indicates one cells. Brain slices from 5 control mice and 5 NVC dysfunction mice. The
1007 data are mean ± s.e.m. N) Fecal production in different transgenic models in 15min OFT. Each
1008 dot indicates one mouse, and the data are mean ± s.e.m. O) Urine map of mice in the OFLT.

P) The presentative heat map of mice trajectory in the OFLT. Q) The urine rate of mice in the OFLT. R) The running distance of mice in the OFLT. Each dot indicates one mouse, and the data are mean ± s.e.m. S) The time of mice speed distribution of mice in the OFLT. Each dot indicates one mouse, and the data are mean ± s.e.m. T) The Log10 ratio between time in right area and the rest of area. Each dot indicates one mouse, and the data are mean ± s.e.m. U) Representative c-fos IF image in the amygdala after the home cage assay. V) The analysis of c-fos activation after the OFT. Each dot indicates the average c-fos expression level of three mice, and the data are mean ± s.e.m. W) The vasculature system distribution in the amygdala. Red signals present blood vessels.

1032 # Tables

1033 **Table 1. List of Mice Genetics**

Common name	Strain name	Resource
Nestin-cre	B6.Cg-Tg(Nes-cre)1Kln/J	Yanmei Tao, Hangzhou Normal University/ Southeast University
Emx1-cre	B6.129S2-Emx1$^{tm1(cre)Krj}$/J	Yanmei Tao, Hangzhou Normal University/ Southeast University
grin2d	B6/JGpt-Grin2d^{em1Cflox}/Gpt	GemPharmatech
SMA-creER	Tg(Acta2-cre/ERT2)12Pcn	Bo Zhou, ShanghaiInstitutes for Biological Sciences, Chinese Academy of Sciences
Ai47	Gt(ROSA)26Sor$^{tm47(CAG-EGFP*)Hze}$	Zilong Qiu, Chinese Academy of Sciences Center for Excellence in Brain Science and Intelligence Technology, Chinese Academy of Sciences.
Pdgfrβ-creER	Tg(Pdgfrb-cre/ERT2)6096Rha	Xiang Yu, Peking University
grin1	*Grin1*^{tm2Stl}	Yangang Sun, Chinese Academy of Sciences Center for Excellence in Brain Science and Intelligence

		Technology, Chinese Academy of Sciences
Ai14	B6.Cg-Gt(ROSA)26Sor$^{tm14(CAG-tdTomato)Hze}$/J	Woo-Ping Ge, Chinese Institute of Brain Research (CIBR)
glrb	C57BL/6JGpt-Glrb^{em1Cflox}/Gpt	GemPharmatech
acta2	C57BL/6JGpt-Acta2^{em1Cflox}/Gpt	GemPharmatech

1034

1035 **Table 2. List of Primer Pairs (Some primers referred to the published PrimerBank**

1036 **database)**

Name		Sequence
grin1	F	AAGAACCTGCAGCAGTACCA
	R	GCAGCAGGACTCATCAGTGT
grin2a	F	TCAGGGACTTTGGAAAACGCT
	R	AAGTCATGCAGGGTTGGTTG
grin2b	F	ACTAACTATCAATGAAGAACGGT
	R	CCAGACCCCAGAGTAACCA
grin2c	F	TGTGGGCCTTCTTCGCTGTCATCT
	R	TGCCATTAGGTACCGTGCCAAAAC

grin2d	F	TGGAGGAGTACGACTGGACAT
	R	CGCACTGACACTACGGAGC
grin3a	F	CTGCACACCAGTCAGAGGTT
	R	TTCGTTGGTTGTCGTGACTC
grin3b	F	TGGGGGTCTACCACTTGTCA
	R	TGGATCTTCTGGCTCGTGTG
ptgs2	F	TTCAACACACTCTATCACTGGC
	R	AGAAGCGTTTGCGGTACTCAT
18s	F	CGGACACGGACAGGATTGACA
	R	CCAGACAAATCGCTCCACCAACTA
cald (siRNA)	S	GUCAAGAGCUUCUUGGAUA
	AS	UAUCCAAGAAGCUCUUGAC

1037

1038 **Table 3. List of Antibodies**

Name	Host	Cat#	Dilution	Company
Anti-NMDAR2D Antibody	Mouse	MAB5578	1:400 (IF) 1:2,500 (WB) 1:1,000 (IP)	Merck

Anti-Smoothelin antibody	Rabbit	ab219652	1:400 (IF)	abcam
α-Smooth Muscle Actin (ACTA2) Rabbit mAb	Rabbit	A17910	1:2,500 (WB)	ABclonal
Anti-NeuN purified Antibody	Guinea Pig	ABN90P	1:800 (IF)	Merck
COX2/PTGS2 Rabbit pAb	Rabbit	A1253	1:400 (IF)	ABclonal
Anti-GLRB antibody	Mouse	EM1710-32	1:400 (IF)	HUABIO
c-Fos antibody	Rabbit	226 003	1:1,000 (IF)	SYSY
Recombinant Alexa Fluor® 488 Anti-Caldesmon/CDM antibody	Rabbit	ab208116	1:400 (IF) 1:2,500 (WB)	abcam
Mice IgG	Mouse	A7028	1:1,000 (IP)	Beyotime
Goat anti-Mouse IgG (H+L) Cross-Adsorbed Secondary Antibody, Alexa Fluor™ 488	Goat	A-11001	1:1,000 (IF)	Invitrogen
Goat anti-Rabbit IgG (H+L) Cross-Adsorbed Secondary Antibody, Alexa Fluor™ 546	Goat	A-11010	1:1,000 (IF)	Invitrogen
Goat anti-Rabbit IgG (H+L) Highly Cross-Adsorbed Secondary Antibody, Alexa Fluor™ 488	Goat	A-11034	1:1,000 (IF)	Invitrogen
Donkey anti-Goat IgG (H+L) Cross-Adsorbed Secondary Antibody, Alexa Fluor™ 647	Donkey	A-21447	1:1,000 (IF)	Invitrogen
Goat Anti-Guinea pig IgG H&L (Alexa Fluor® 488)	Goat	ab150185	1:1,000 (IF)	abcam

Goat Anti-Guinea pig IgG H&L (Alexa Fluor® 555)	Goat	ab150186	1:1,000 (IF)	abcam
β-Tubulin Mouse mAb	Mouse	AC021	1:5,000 (WB)	ABclonal
Goat Anti-Mouse IgG, HRP Conjugated	Goat	CW0102	1:10,000 (WB)	CWBIO
Goat Anti-Rabbit IgG, HRP Conjugated	Goat	CW0103	1:10,000 (WB)	CWBIO

Data availability

The code is available at https://github.com/JialabEleven/ with citation. Another data is available from authors upon reasonable request.

Author contributions

Jie-Min Jia conceived the project, designed the experiments, and supervised this study. Jiayu Ruan designed mice management, operated all major assay, obtained all major original data, and wrote the manuscript. Huiqi Xie participated in blood pressure measurement, long-term whisker stimulation, and behavioral assay. Xinghua Quan made *cald* siRNA interference assay, and participated behavioral assay. Yiyi Zhang wrote main MATLAB code. Dongdong Zhang provided primer pairs of *grin1* and provided suggestions. Wentao Wang participated in the writing of MATLAB code.

Figure1

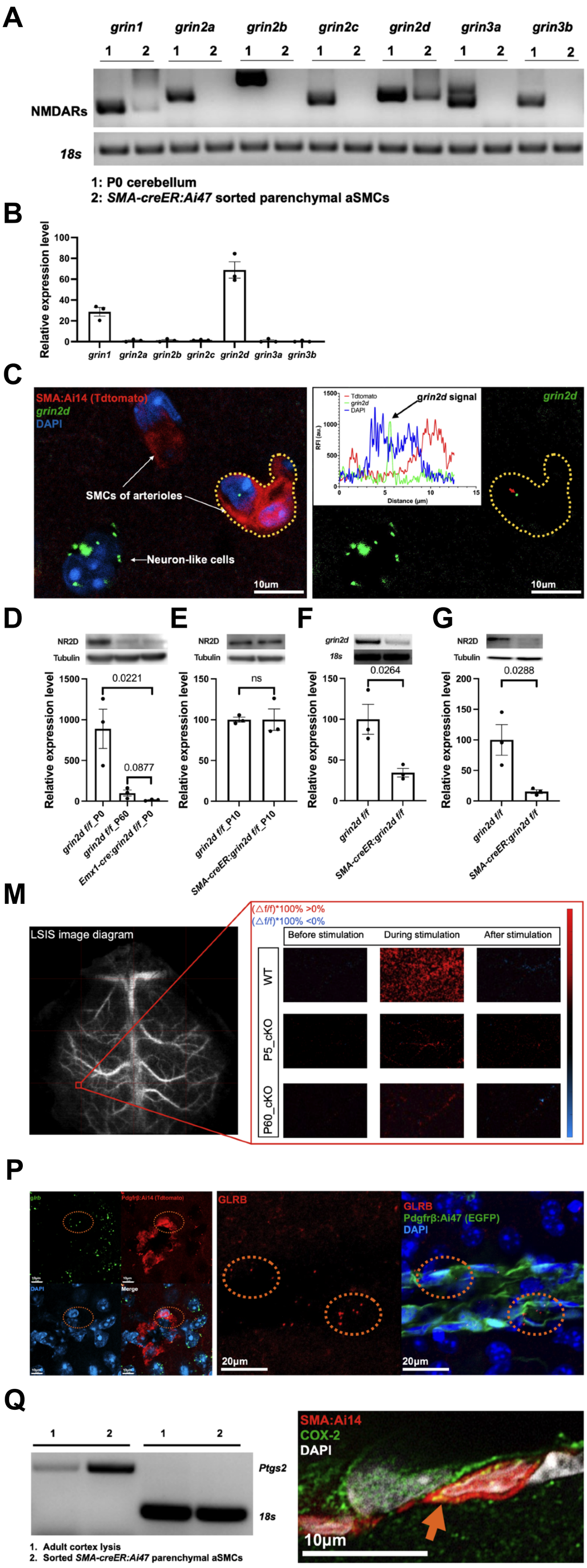
A
grin1 grin2a grin2b grin2c grin2d grin3a grin3b
NMDARs
18s
1: P0 cerebellum
2: SMA-creER:Ai47 sorted parenchymal aSMCs
B
Relative expression level
C
SMA:Ai14 (Tdtomato)
grin2d
DAPI
SMCs of arterioles
Neuron-like cells
grin2d signal
10μm
D
E
F
G
NR2D
Tubulin
0.0221
0.0877
ns
0.0264
0.0288
Relative expression level
grin2d f/f_P0
grin2d f/f_P60
Emx1-cre:grin2d f/f_P0
grin2d f/f_P10
SMA-creER:grin2d f/f_P10
grin2d f/f
SMA-creER:grin2d f/f
M
LSIS image diagram
(△f/f)*100% >0%
(△f/f)*100% <0%
Before stimulation
During stimulation
After stimulation
WT
P5_cKO
P60_cKO
P
GLRB
Pdgfrβ:Ai47 (EGFP)
DAPI
20μm
Q
Ptgs2
18s
1. Adult cortex lysis
2. Sorted SMA-creER:Ai47 parenchymal aSMCs
SMA:Ai14
COX-2
DAPI
10μm
H
Smoothelin
NR2D
DAPI
10μm
EGFP
NR2D
5μm
I
J
K
L
SMA
Tubulin
****
ns
0.0003
grin2d f/f
SMA-creER:grin2d f/f
N
Stimulation (12Hz)
CBF Variation (%)
Seconds
Littermate control mice
SMA-creER:grin2d f/f_P5
SMA-creER:grin2d f/f_P60
SMA-creER::ptgs2 f/f
SMA-creER:grin2d f/f:grin1 f/f
Pdgfrβ-creER:grin2d f/f
Pdgfrβ-creER:glrb f/f
Emx1-cre:ptgs2 f/f
O
CBF Variation (%) / Seconds
Peak mean (%)
Time to peak (s)
R
S
T
Number of signal dots per cell
0.2202
Number of signal dots per μm
0.0040
Relative expression level
0.0014
aSMCs
Pericyte
vSMCs
Arterioles
Venules
Cortex lysis

Figure2

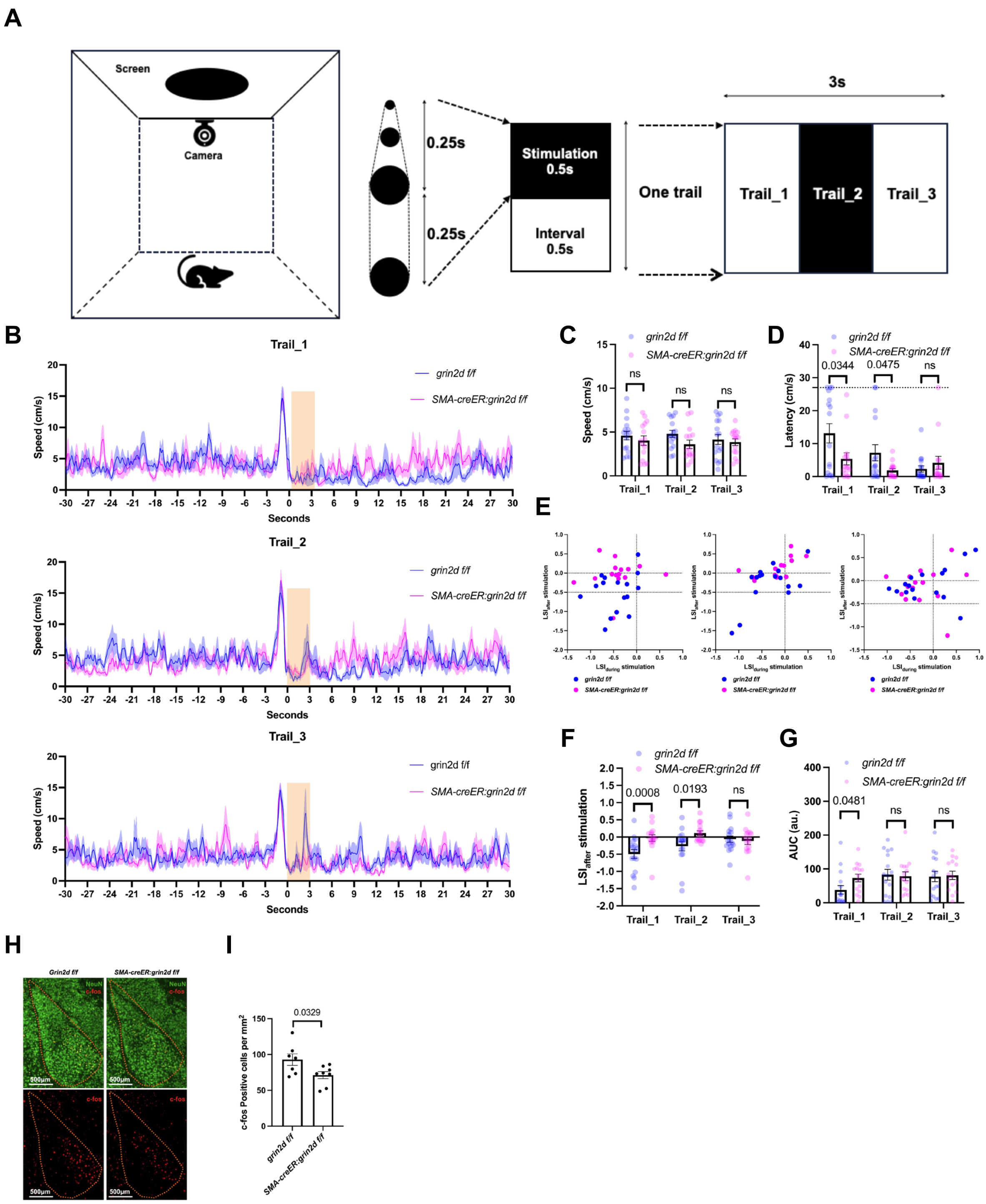
A
Screen
Camera
0.25s
0.25s
Stimulation 0.5s
Interval 0.5s
One trail
3s
Trail_1
Trail_2
Trail_3
B
Trail_1
Trail_2
Trail_3
grin2d f/f
SMA-creER:grin2d f/f
Speed (cm/s)
Seconds
C
Speed (cm/s)
ns
D
Latency (cm/s)
0.0344
0.0475
E
LSI after stimulation
LSI during stimulation
F
0.0008
0.0193
G
AUC (au.)
0.0481
H
Grin2d f/f
SMA-creER:grin2d f/f
NeuN
c-fos
500μm
I
c-fos Positive cells per mm2
0.0329

Figure3

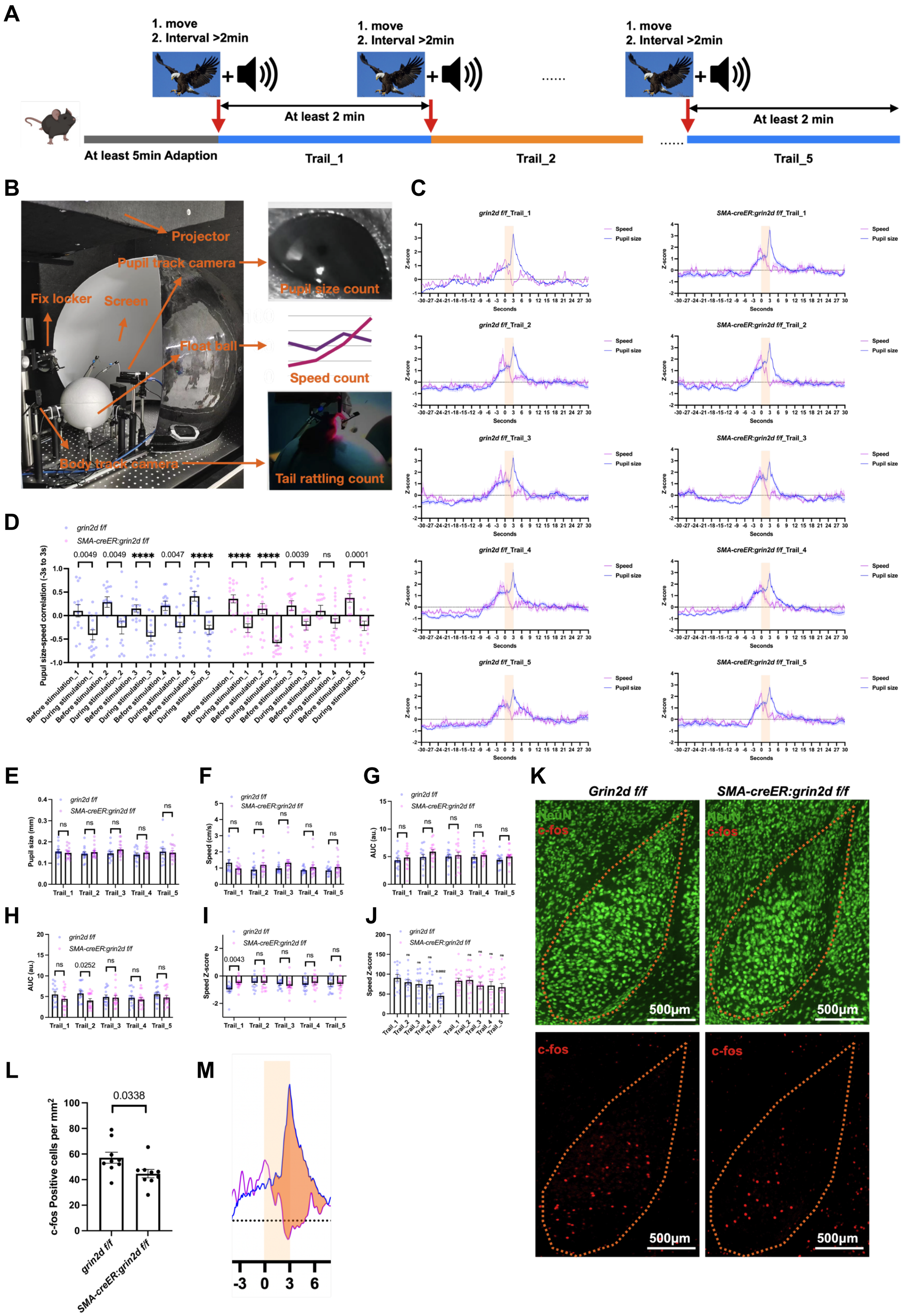
A
1. move
2. Interval >2min
At least 2 min
At least 5min Adaption
Trail_1
Trail_2
Trail_5
B
Projector
Pupil track camera
Fix locker
Screen
Float ball
Body track camera
Pupil size count
Speed count
Tail rattling count
C
grin2d f/f_Trail_1
SMA-creER:grin2d f/f_Trail_1
Speed
Pupil size
Z-score
Seconds
D
grin2d f/f
SMA-creER:grin2d f/f
Pupil size-speed correlation (-3s to 3s)
E
Pupil size (mm)
F
Speed (cm/s)
G
AUC (au.)
H
AUC (au.)
I
Speed Z-score
J
Speed Z-score
K
Grin2d f/f
SMA-creER:grin2d f/f
NeuN
c-fos
500μm
L
c-fos Positive cells per mm²
0.0338
grin2d f/f
SMA-creER:grin2d f/f
M

Figure4

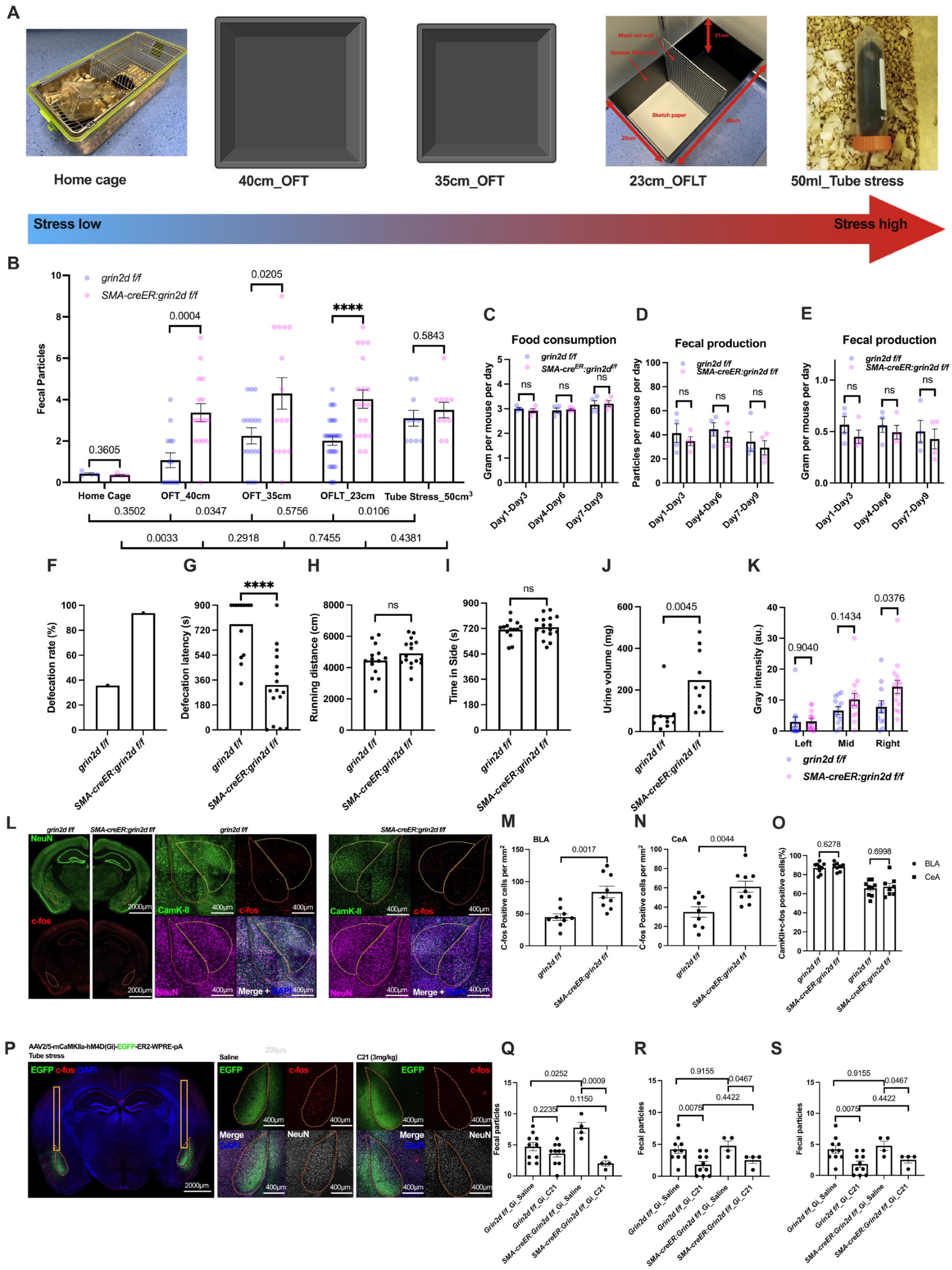
A
Home cage
40cm_OFT
35cm_OFT
23cm_OFLT
50ml_Tube stress
Stress low
Stress high
B
grin2d f/f
SMA-creER:grin2d f/f
Fecal Particles
Home Cage
OFT_40cm
OFT_35cm
OFLT_23cm
Tube Stress_50cm³
C
Food consumption
D
Fecal production
E
Fecal production
Day1-Day3
Day4-Day6
Day7-Day9
F
Defecation rate (%)
G
Defecation latency (s)
H
Running distance (cm)
I
Time in Side (s)
J
Urine volume (mg)
K
Gray intensity (au.)
Left
Mid
Right
L
NeuN
c-fos
CamK-II
Merge + DAPI
M
BLA
C-fos Positive cells per mm²
N
CeA
O
CamKII+c-fos positive cells(%)
P
AAV2/5-mCaMKIIa-hM4D(Gi)-EGFP-ER2-WPRE-pA
Tube stress
Saline
C21 (3mg/kg)
EGFP
Merge
DAPI
Q
R
S
Fecal particles
Grin2d f/f_Gi_Saline
Grin2d f/f_Gi_C21
SMA-creER:Grin2d f/f_Gi_Saline
SMA-creER:Grin2d f/f_Gi_C21

Figure S1

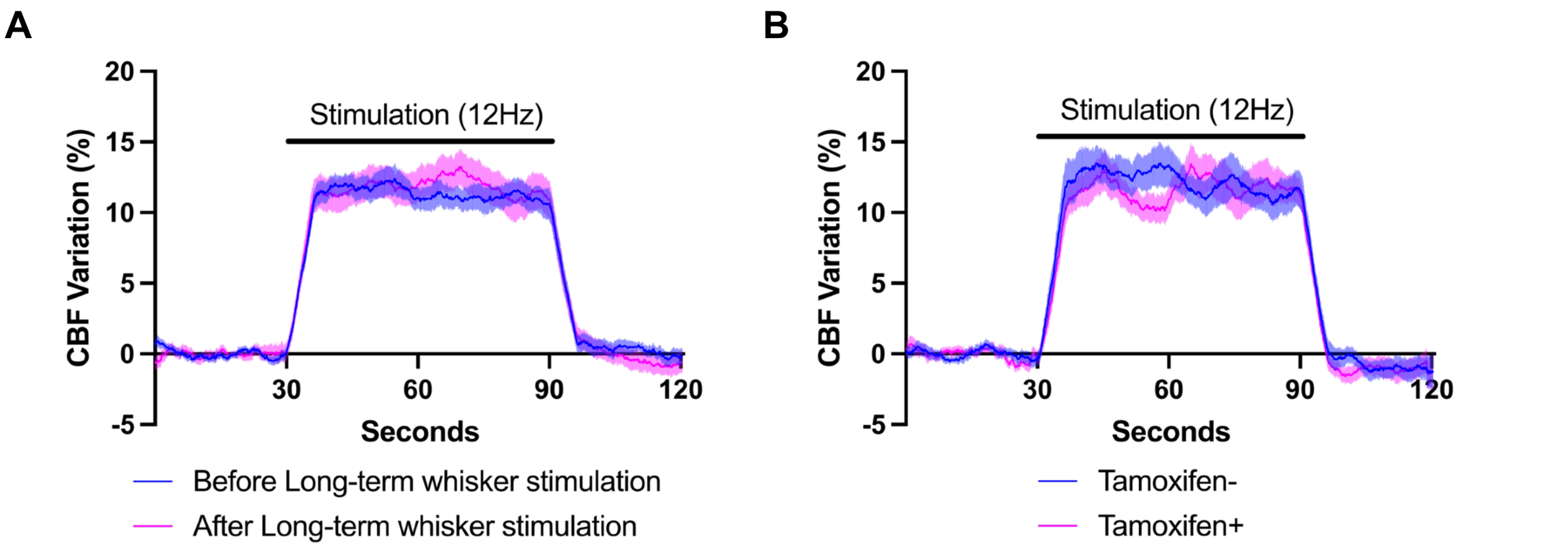
A
B
Stimulation (12Hz)
CBF Variation (%)
Seconds
Before Long-term whisker stimulation
After Long-term whisker stimulation
Tamoxifen-
Tamoxifen+

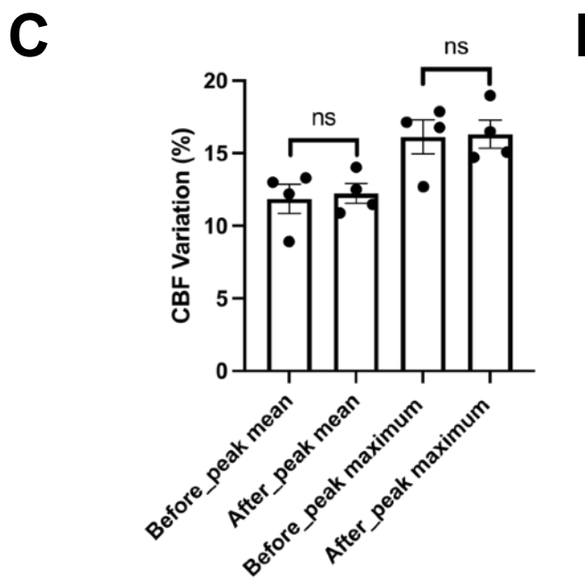
C
ns
CBF Variation (%)
Before_peak mean
After_peak mean
Before_peak maximum
After_peak maximum

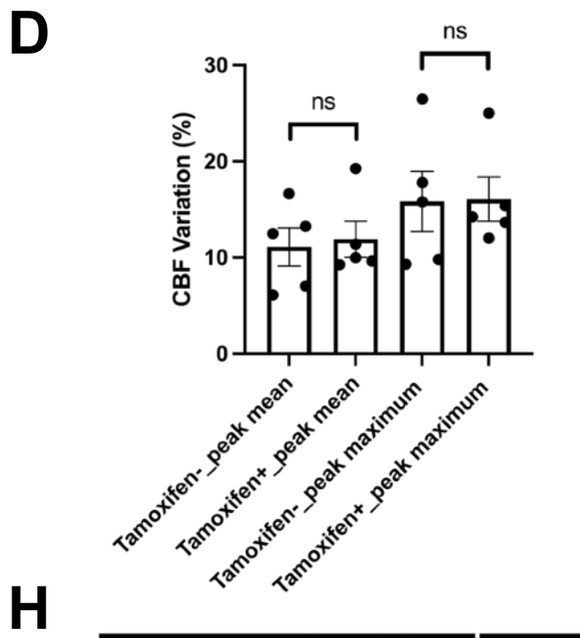
D
ns
CBF Variation (%)
Tamoxifen-_peak mean
Tamoxifen+_peak mean
Tamoxifen-_peak maximum
Tamoxifen+_peak maximum

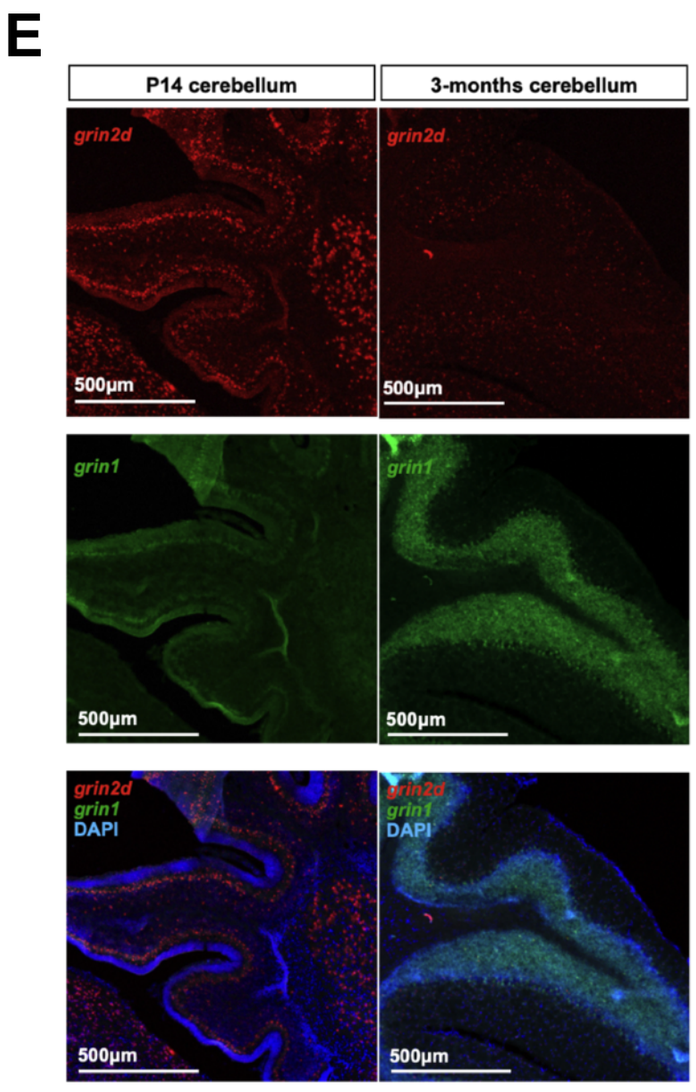
E
P14 cerebellum
3-months cerebellum
grin2d
grin1
DAPI
500µm

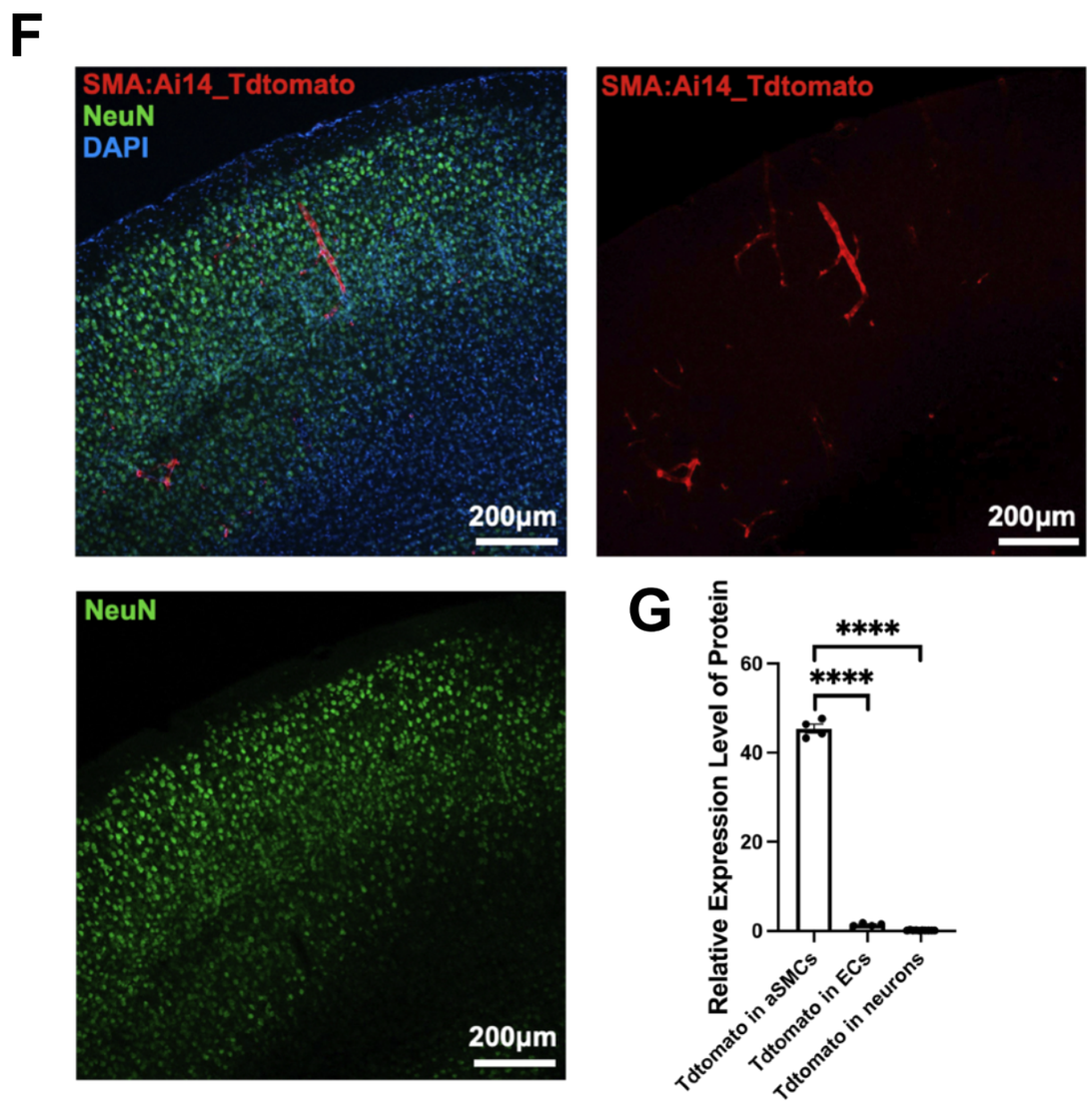
F
SMA:Ai14_Tdtomato
NeuN
DAPI
200µm
G
Relative Expression Level of Protein
****
Tdtomato in aSMCs
Tdtomato in ECs
Tdtomato in neurons

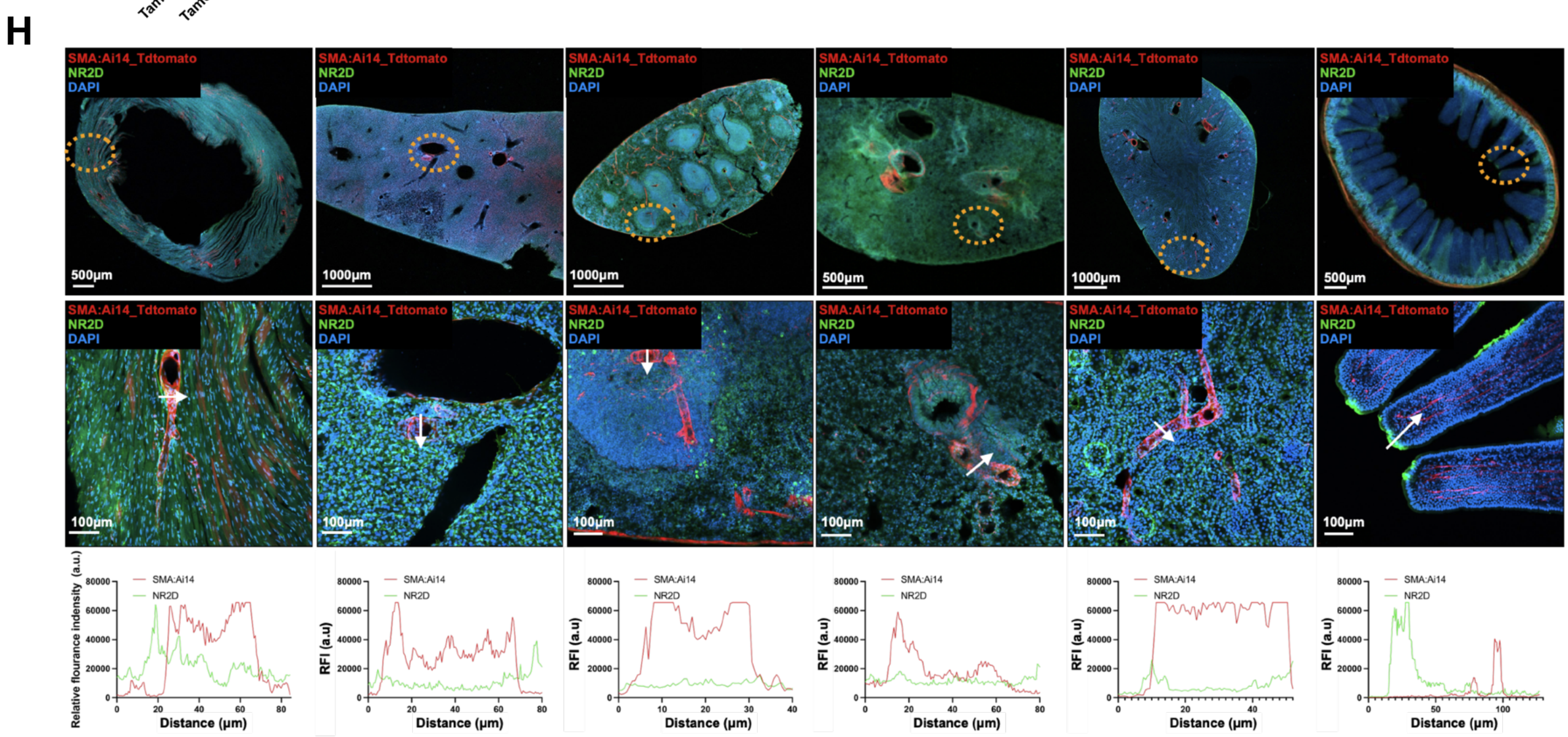
H
SMA:Ai14_Tdtomato
NR2D
DAPI
500µm
1000µm
100µm
Relative flourance indensity (a.u.)
RFI (a.u)
SMA:Ai14
NR2D
Distance (µm)

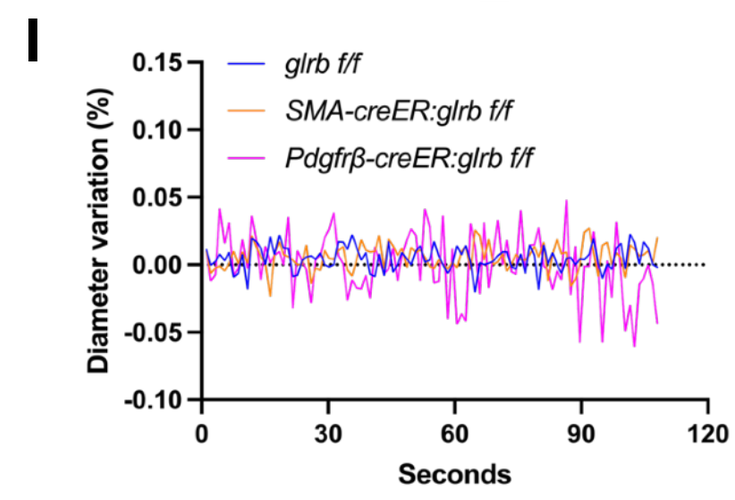
I
glrb f/f
SMA-creER:glrb f/f
Pdgfrβ-creER:glrb f/f
Diameter variation (%)
Seconds

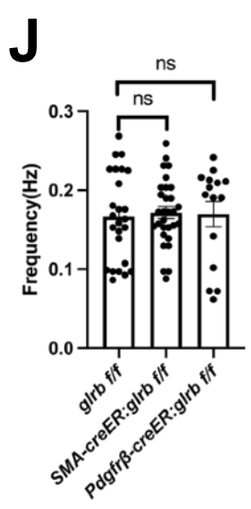
J
ns
Frequency(Hz)
glrb f/f
SMA-creER:glrb f/f
Pdgfrβ-creER:glrb f/f

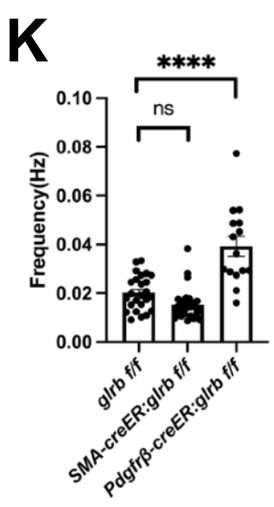
K
****
ns
Frequency(Hz)
glrb f/f
SMA-creER:glrb f/f
Pdgfrβ-creER:glrb f/f

Figure S2

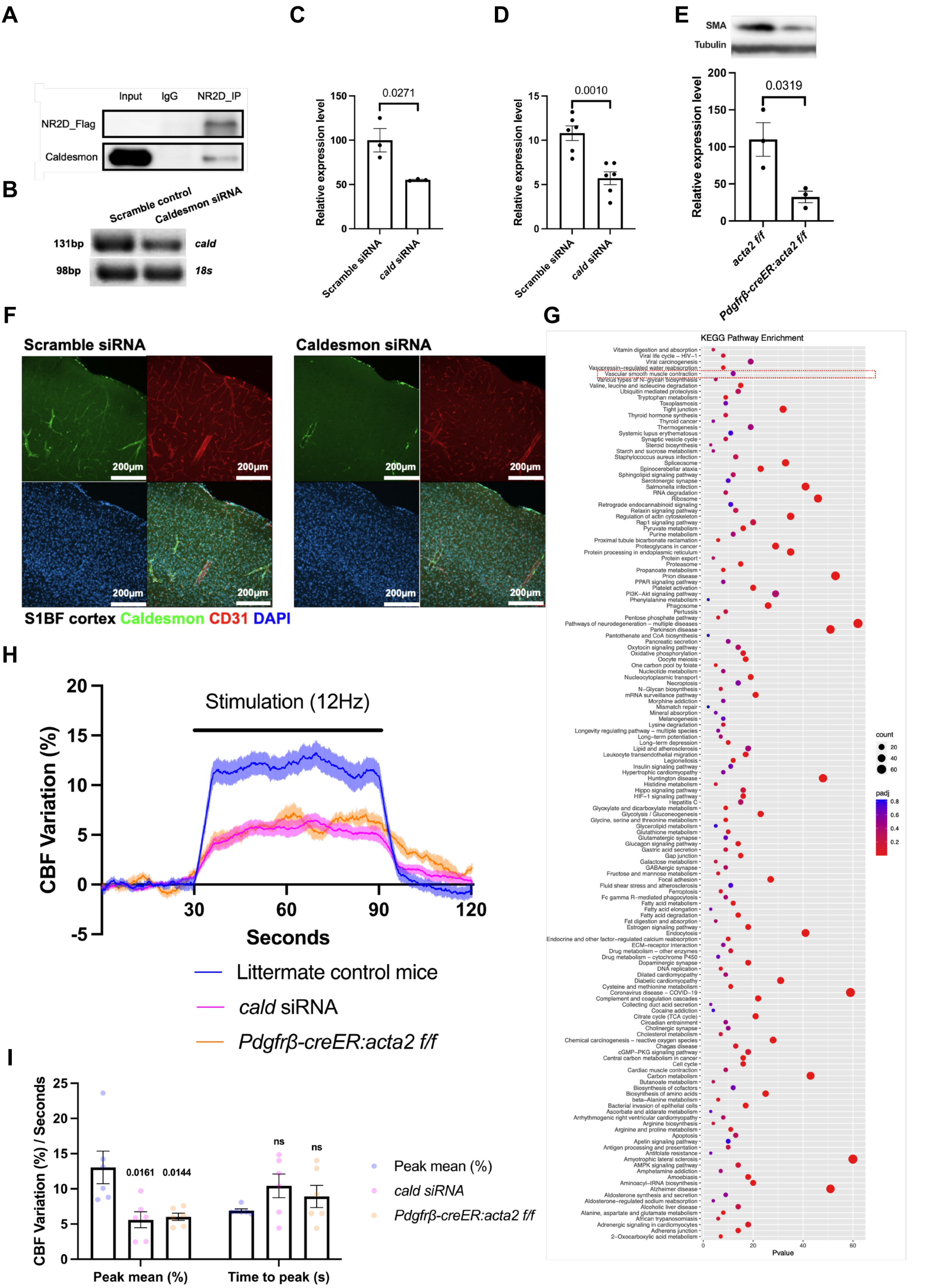
A
Input
IgG
NR2D_IP
NR2D_Flag
Caldesmon
B
Scramble control
Caldesmon siRNA
131bp
98bp
cald
18s
C
Relative expression level
0.0271
Scramble siRNA
cald siRNA
D
Relative expression level
0.0010
Scramble siRNA
cald siRNA
E
SMA
Tubulin
Relative expression level
0.0319
acta2 f/f
Pdgfrβ-creER:acta2 f/f
F
Scramble siRNA
Caldesmon siRNA
200μm
S1BF cortex Caldesmon CD31 DAPI
G
KEGG Pathway Enrichment
count
padj
Pvalue
H
Stimulation (12Hz)
CBF Variation (%)
Seconds
Littermate control mice
cald siRNA
Pdgfrβ-creER:acta2 f/f
I
CBF Variation (%) / Seconds
0.0161
0.0144
ns
ns
Peak mean (%)
Time to peak (s)
Peak mean (%)
cald siRNA
Pdgfrβ-creER:acta2 f/f

Figure S3

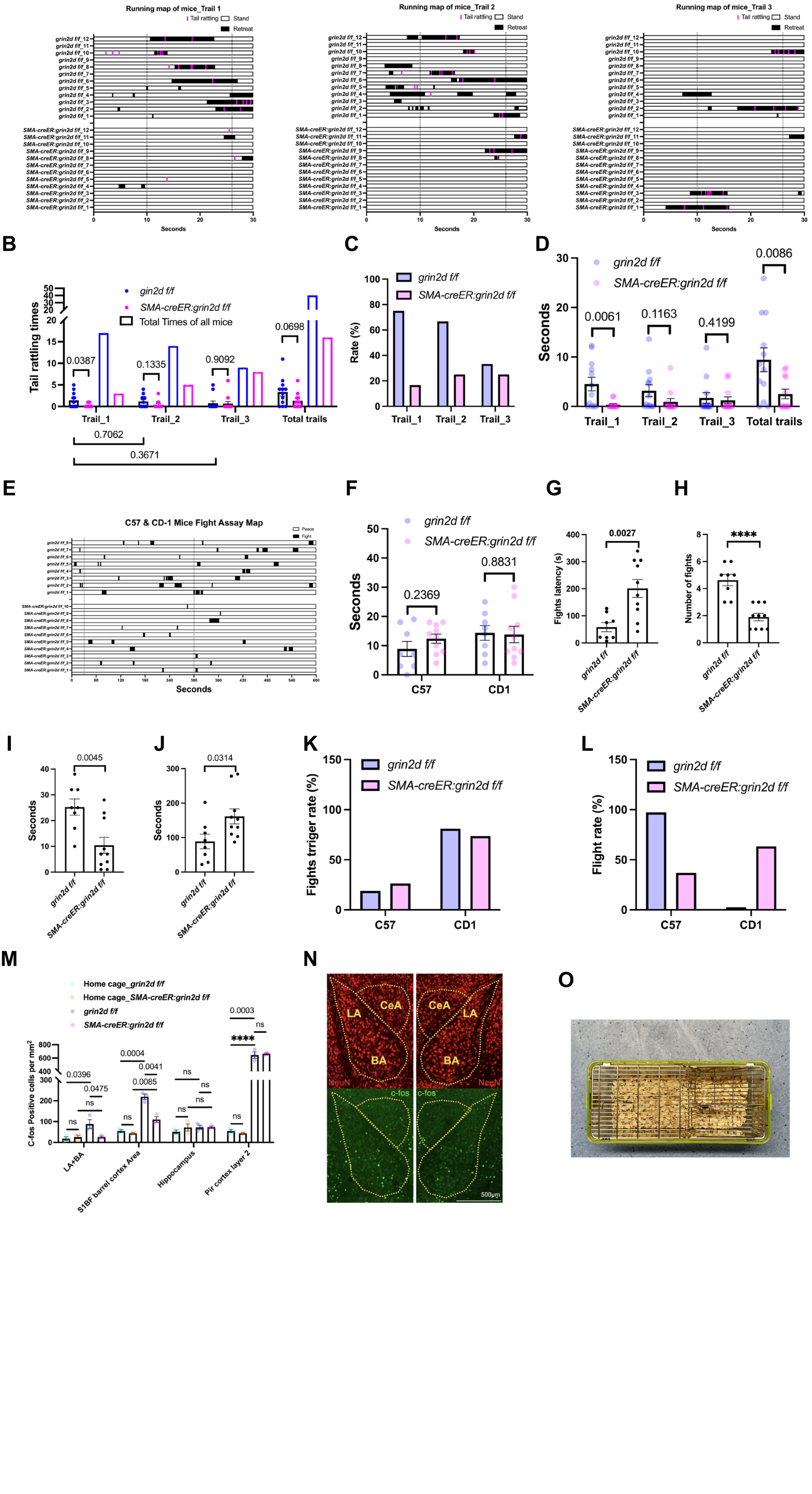
A
Running map of mice_Trail 1
Running map of mice_Trail 2
Running map of mice_Trail 3
Tail rattling
Stand
Retreat
Seconds
B
Tail rattling times
gin2d f/f
SMA-creER:grin2d f/f
Total Times of all mice
0.0387
0.1335
0.9092
0.0698
Trail_1
Trail_2
Trail_3
Total trails
0.7062
0.3671
C
Rate (%)
D
Seconds
0.0061
0.1163
0.4199
0.0086
E
C57 & CD-1 Mice Fight Assay Map
Peace
Fight
F
0.2369
0.8831
C57
CD1
G
Fights latency (s)
0.0027
H
Number of fights
****
I
0.0045
J
0.0314
K
Fights trriger rate (%)
L
Flight rate (%)
M
Home cage_grin2d f/f
Home cage_SMA-creER:grin2d f/f
C-fos Positive cells per mm²
LA+BA
S1BF barrel cortex Area
Hippocampus
Pir cortex layer 2
N
LA
CeA
BA
NeuN
c-fos
500μm
O

Figure S4

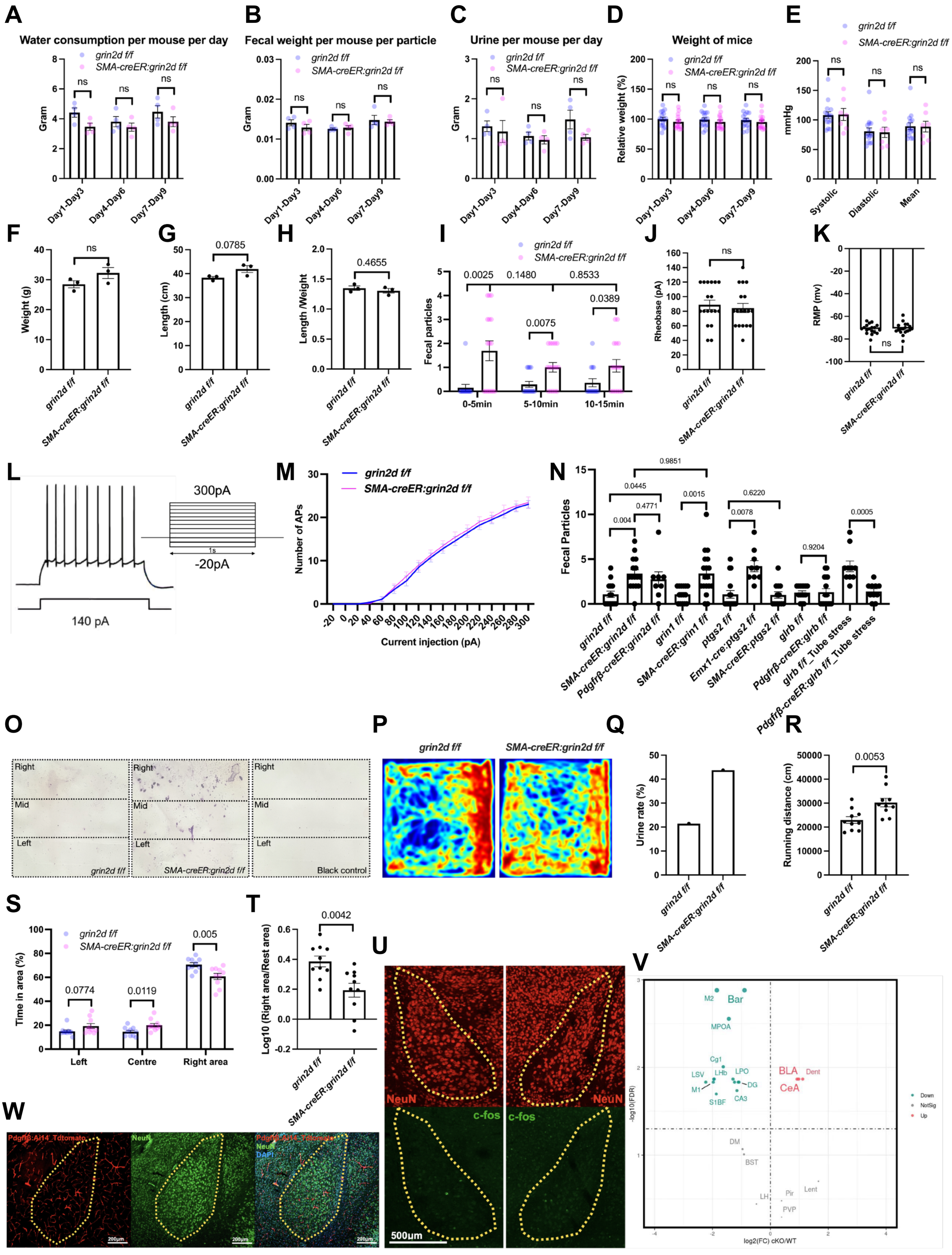
A
Water consumption per mouse per day
grin2d f/f
SMA-creER:grin2d f/f
Gram
ns
Day1-Day3
Day4-Day6
Day7-Day9
B
Fecal weight per mouse per particle
C
Urine per mouse per day
D
Weight of mice
Relative weight (%)
E
mmHg
Systolic
Diastolic
Mean
F
Weight (g)
G
Length (cm)
0.0785
H
Length /Weight
0.4655
I
Fecal particles
0.0025
0.1480
0.8533
0.0389
0.0075
0-5min
5-10min
10-15min
J
Rheobase (pA)
K
RMP (mv)
L
300pA
-20pA
1s
140 pA
M
Number of APs
Current injection (pA)
N
Fecal Particles
0.9851
0.0445
0.4771
0.004
0.0015
0.6220
0.0078
0.9204
0.0005
grin2d f/f
SMA-creER:grin2d f/f
Pdgfrβ-creER:grin2d f/f
grin1 f/f
SMA-creER:grin1 f/f
ptgs2 f/f
Emx1-cre:ptgs2 f/f
SMA-creER:ptgs2 f/f
glrb f/f
Pdgfrβ-creER:glrb f/f
glrb f/f_Tube stress
Pdgfrβ-creER:glrb f/f_Tube stress
O
Right
Mid
Left
Black control
P
Q
Urine rate (%)
R
Running distance (cm)
0.0053
S
Time in area (%)
0.0774
0.0119
0.005
Left
Centre
Right area
T
Log10 (Right area/Rest area)
0.0042
U
NeuN
c-fos
500μm
V
M2
Bar
MPOA
Cg1
LSV
LHb
LPO
M1
DG
S1BF
CA3
BLA
Dent
CeA
DM
BST
LH
Pir
Lent
PVP
-log10(FDR)
log2(FC) cKO/WT
Down
NotSig
Up
W
Pdgfrβ:Ai14_Tdtomato
NeuN
DAPI
200μm